LEBANESE AMERICAN UNIVERSITY

Approximate Differentiator with Varying Bandwidth

By

Rayana Hussein Jaafar

A thesis
Submitted in partial fulfillment of the requirements
for the degree of Master of Science in Computer Engineering

School of Engineering
July 2019

LAU
الجامعة اللبنانية الأميركية
Lebanese American University

THESIS APPROVAL FORM

Student Name: Royana yaafar I.D. #: 201205238

Thesis Title: Approximate Differentiator with Varying Bandwidth

Program: Master of Science in Computer Engineering

Department: Department of Electrical and Computer Engineering

School: School of Engineering

The undersigned certify that they have examined the final electronic copy of this thesis and approved it in Partial Fulfillment of the requirements for the degree of:

Master of Science in the major of Computer Engineering

Thesis Advisor's Name: [redacted]

Signature: [redacted] Date: 4 / 7 / 2019 (Day / Month / Year)

Committee Member's Name: Dani Tannir

Signature: [redacted] Date: 4 / 7 / 2019 (Day / Month / Year)

Committee Member's Name: Zaki Nakad

Signature: [redacted] Date: 4 / 7 / 19 (Day / Month / Year)

LAU
الجامعة اللبنانية الأميركية
Lebanese American University

THESIS COPYRIGHT RELEASE FORM

LEBANESE AMERICAN UNIVERSITY NON-EXCLUSIVE DISTRIBUTION LICENSE

By signing and submitting this license, you (the author(s) or copyright owner) grants the Lebanese American University (LAU) the non-exclusive right to reproduce, translate (as defined below), and/or distribute your submission (including the abstract) worldwide in print and electronic formats and in any medium, including but not limited to audio or video. You agree that LAU may, without changing the content, translate the submission to any medium or format for the purpose of preservation. You also agree that LAU may keep more than one copy of this submission for purposes of security, backup and preservation. You represent that the submission is your original work, and that you have the right to grant the rights contained in this license. You also represent that your submission does not, to the best of your knowledge, infringe upon anyone's copyright. If the submission contains material for which you do not hold copyright, you represent that you have obtained the unrestricted permission of the copyright owner to grant LAU the rights required by this license, and that such third-party owned material is clearly identified and acknowledged within the text or content of the submission. IF THE SUBMISSION IS BASED UPON WORK THAT HAS BEEN SPONSORED OR SUPPORTED BY AN AGENCY OR ORGANIZATION OTHER THAN LAU, YOU REPRESENT THAT YOU HAVE FULFILLED ANY RIGHT OF REVIEW OR OTHER OBLIGATIONS REQUIRED BY SUCH CONTRACT OR AGREEMENT. LAU will clearly identify your name(s) as the author(s) or owner(s) of the submission, and will not make any alteration, other than as allowed by this license, to your submission.

Name: Rayana Jaafar

Signature: [redacted]

Date: 4 / 7 / 19
Day Month Year

LAU
الجامعة اللبنانية الأميركية
Lebanese American University

PLAGIARISM POLICY COMPLIANCE STATEMENT

I certify that:

1. I have read and understood LAU's Plagiarism Policy.
2. I understand that failure to comply with this Policy can lead to academic and disciplinary actions against me.
3. This work is substantially my own, and to the extent that any part of this work is not my own I have indicated that by acknowledging its sources.

Name: Rayana Jaafar

Signature: [redacted]

Date: 4 / 7 / 19
Day / Month / Year

ACKNOWLEDGMENT

Foremost, I would like to start by expressing my sincere thanks to my advisor, Professor Samer S. Saab. His endless support, motivation, enthusiasm, patience and outstanding knowledge has been shaping my way at all times.

I would also like to extend my sincere gratitude to the dear members of my thesis committee, Dr. Zahi Nakad and Dr. Dani Tannir. Their continuous guidance and encouragement have added invaluable knowledge to my graduate experience.

To my friends, thank you for being around through the good and bad. This long process has been much easier with your continuous support and faith in me.

Finally, to my family, I did it all for you and because of you. Nothing would have been possible without the care and love you have always given me.

Approximate Differentiator with Varying Bandwidth

Rayana Hussein Jaafar

ABSTRACT

In the 1960's, innovative research in the former Soviet Union laid grounds for the evolution of the Sliding Mode Control (SMC). Known for its robustness and insensitivity to parameter variations, SMC immediately became an efficient tool for the control of highly non-linear systems, such as rigid robot manipulators. Despite its significant advantages, SMC was criticized for an inherent drawback manifested by the chattering phenomenon. The latter may cause vibrations that could eventually compromise the safety of the manipulator as well as degrade its tracking performance. In its simplest form, SMC requires measurements of joint positions and velocities as the terminal sliding variable vector has a non-linear term of both joint positions and velocities. Since most industrial manipulators are not equipped with velocity sensors, typical SMC applications resort to different methodologies to approximate joint velocities from measurements of joint positions. The Approximate Differentiator, also referred to as the Dirty Derivatives Filter (DF), is a first order filter that estimates the joint velocity *error* commonly used in feedback control. In this thesis, we exploit key differences between the continuous-time model of the DF and its discrete-time model. We show that the discrete-time filter shares the characteristics of an exponentially weighted moving average; in particular, the filter *smooths* the derivative of its input. We integrate the discrete-time DF with a conventional SMC and show the stability of

the closed-loop system. We numerically and experimentally demonstrate how the filter estimation performance follows a *convex trend* in function of the filter bandwidth. We further demonstrate how the bandwidth at which the filter achieves "*optimal*" performance varies with the *frequency* of the filter input. Inspired by the latter, we propose an Approximate Differentiator with Varying Bandwidth (ADVB) where the filter bandwidth varies based on the magnitude of the position tracking error. We illustrate the superiority of the proposed ADVB over the "optimal" DF numerically and experimentally on a four-degree-of-freedom (DOF) robot manipulator. We also demonstrate that DF outperforms a High-Gain Observer for the closed-loop control system under consideration.

Keywords: Approximate Differentiator, Dirty-Derivatives Filter, Velocity Estimation, Sliding Mode Control, Robot Manipulator.

Table of Contents

List of Tables

List of Figures

Chapter 1

Introduction

1.1 Sliding Mode Control

In the 1960's, innovative research in the former Soviet Union laid grounds for the evolution of the Sliding Mode Control (SMC) [1, 2, 3, 4]. Due to its fast-dynamic responses, external disturbance rejection [5, 6], and insensitivity to parameter variations [7, 8], SMC is nowadays considered a powerful method for the control of high-order non-linear systems, such as rigid robotic manipulators [9, 10].

In the presence of large uncertainties and disturbances, the employment of relatively high control gain causes the SMC to amplify input and output disturbances which eventually leads to high-frequency chattering [11] and fast-switching control phenomena [12, 13]. Various effective methods have been proposed in an attempt to reduce the chattering problem such as higher order control [14, 15, 16], low-pass filtering [17, 18], boundary layer setting [19, 20], and adaptive sliding mode control [21, 22, 23]. In general, SMC requires measurements of joint positions and velocities since the terminal sliding variable vector has a nonlinear term of the position and velocity error [24, 25, 26]. Although joint position measurements can be easily

acquired with good precision encoders, the ability to measure joint velocities remains an issue due to the significance of the measurement noise [27, 28, 29]. While also considering the involved cost, it follows that most industrial robots are not equipped with velocity sensors [30]. For SMC, the estimation of joint velocities is critical since inaccurate or even non-smooth velocity estimation may cause input and output chattering or instability of the closed-loop control system [31].

1.2 Joint Velocity Estimation Techniques

The literature is swamped with proposed methods to estimate the joint velocities from the measurements of the joint positions. In what follows, we list the techniques commonly used for the approximation of joint velocities.

One of the most popular techniques for velocity approximation is based on directly processing the discrete-time joint position measurements such as Euler-difference method [32, 33] and adaptive windowing method [34, 35]. However, the resulting estimates may be highly erroneous especially at low-velocity ranges where the encoder output rate is correspondingly low [36, 37]. Typically, an optical encoder yields quantization errors which highly depend on the encoder resolution [38]. As a result, velocity signals that are approximated using Euler-discretization are contaminated with high-frequency noise [39, 40]. This may cause the controller to excite unmodeled high-frequency dynamics which could further deteriorate the accuracy of position control [41]. In order to avoid the latter, filters are typically employed in an attempt to smooth the position signal before discretization. Due to their simple implementation, linear filters are widely used to attenuate the noisy components of the measured position signal. However, such filters may cause a large phase delay which could be

problematic for the stability of the feedback loop. To mitigate the latter drawbacks, non-linear filters are sometimes used to remove the high-frequency components at the cost of implementation complexity and additional computational time [39]. In [34], authors present a first-order adaptive windowing method to estimate velocity from discrete and quantized position samples. The proposed approach is shown to be optimal in the sense that it maximizes the estimation accuracy while minimizing the error variance. However, despite requiring no trade-off, the proposed method's computational cost is dependent on the window size as well as the sampling rate.

Another approach deals with the implementation of a velocity observer, which can be generally classified into two types: model-based and model-free observers. Model-based observers assume some knowledge of the system model, which could be problematic in the presence of large model uncertainties [42]. In addition, since the certainty principle does not generally apply for non-linear systems, the design of such observers becomes a challenging task. On the other hand, model-free observers, such as High-Gain Observers (HGO) [43] do not require a knowledge of the system model. In [44], a HGO with a switched-gain approach is proposed for a class of non-linear systems in the presence of measurement noise. In [45], a non-linear HGO where nonlinearity achieves a higher observer gain during the transient period and a lower gain after is presented. Theoretically, and in the absence of measurement noise, the estimation errors of the HGO tend to zero as the observer gain grows to infinity. The latter does not hold in the presence of measurement noise since the high-gain nature of the observer leads to the amplification of noise in the resulting signal which could deteriorate the overall system performance. It follows that there exists a trade-off between the HGO estimation accuracy and the amount of noise amplification. The

latter renders the design and tuning of a HGO challenging since the choice of observer parameters is critical in a way such that the values should not be too small nor too large [46]. Having a more complicated implementation than the latter, High-Oder Sliding Mode (HOSM) observers generally require minimal knowledge of the system model such as the relative degree. In [47], an adaptation of Levant's differentiator where the gains are adjusted based on a barrier function is proposed. The latter pushes the differentiator gains towards infinity whenever the estimation of the considered signal is beyond a given band. In [48], a Lyapunov function is presented for Levant's differentiator, where the differentiator gains are assumed to depend on a known time-varying function which bounds the n^{th} derivative of the considered signal.

Another common class for obtaining high quality velocity estimations is based on filtering techniques such as approximate-differentiation filter [49], non-linear filter [50], and model-free Kalman filter [51].

1.3 Problem Formulation

In tracking control applications, the advantage of the latter methods lies in the ability to perform tuning in an offline fashion based on the specific reference trajectories under consideration while implicitly assuming acceptable uniform tracking performance of the controller. Despite such merit, these methods suffer from one major drawback where the output can change abruptly due to unmodeled dynamics such as joint friction [52]. This could lead to unknown jumps in the estimated velocity signal where the bandwidth becomes significantly greater than the one associated with the reference trajectories leading to poor tracking performance of the SMC as well as non-smooth joint torques [53] [54]. Of note, if such methods are tuned for trajectories with

arbitrary large bandwidth, then the estimation may suffer unavoidable overshoots that can destabilize the closed-loop system. The Approximate Differentiator filter, also commonly known as the Dirty Derivatives Filter (DF), is a first order filter that estimates the joint velocity *error* commonly used in feedback control [55]. In [56], a DF is integrated with a PD-Type controller where uniform global asymptotic stability is established while only a lower bound on the filter bandwidth is imposed. However, the tuning process of the DF within the closed-loop control system remains challenging as the tuning imposes a constraint on the derivative damping gain scaled by the DC gain of the filter [56]. Although the DF has been used with feedback controllers (see, e.g., the relevant references in [56] and [30]), its characteristics have never been thoroughly studied.

1.4 Contribution

In this thesis, we first examine the characteristics of the DF. We reflect on how the discretized version of the filter, required for digital control applications, differs from its analog model. In particular, unlike the analog filter, the discrete filter bandwidth cannot be made arbitrarily large. We also show that the output of the DF is a "*smoothed*" version of the estimated joint velocity error, where the filter shares the smoothing characteristics of an Exponentially Weighted Moving Average (EWMA). This characteristic has a critical advantage in control tracking applications where non-smooth estimations of joint velocity can potentially lead to strong vibrations in the arm. The latter issue is illustrated by comparing the SMC tracking performance while using a DF versus a HGO. We show the stability of the SMC-DF closed-loop system. Furthermore, using a sinusoidal test signal with a fixed frequency, we show that the *estimation performance* of the DF follows a *convex* trend in function of its bandwidth

or location of its pole. In addition, we show that as the frequency of the input signal varies, the filter bandwidth at which the DF achieves the lowest estimation error also varies. In control tracking applications, the actual frequency of the position signal constantly varies, for example, during transient response or due to unmodeled disturbances. As a result, the "optimal" DF bandwidth at which the tracking error is the lowest also varies. In order to preserve the "optimal" DF performance, we propose an Approximate Differentiator filter with Varying Bandwidth (ADVB) where the filter bandwidth varies based on the joint position error. The adopted premise is based on the following concept: As the tracking error decreases, the frequency deviation of the position output also decreases. We then illustrate the effectiveness of the proposed filter numerically and experimentally on a 4 DoF Barret WAM manipulator which generally suffers from frictional joint torques [30].

The main contributions of this thesis are as follows:

- We study the characteristics of the discrete-time DF and show that the filter smooths the derivative of its input.
- We integrate the DF with a conventional SMC and show stability of the closed loop.
- We demonstrate that the DF outperforms the HGO when integrated with an SMC while considering both joint tracking error and joint torques.
- We numerically and experimentally show how the estimation performance of the DF follows a convex trend in function of its bandwidth.
- Inspired by the latter point, we propose an Approximate Differentiator with Varying Bandwidth (ADVB) where the filter bandwidth constantly varies based on the position tracking errors in order to preserve the "optimal" filter

performance. We validate the performance superiority of the proposed filter both numerically and experimentally.

The rest of the thesis is arranged as follows:

- Chapter 2 presents analysis of the characteristics of the discrete-time DF
- Chapter 3 presents stability analysis of the SMC-DF closed-loop control system
- Chapter 4 presents an adaptation law for the filter bandwidth
- Chapter 5 presents numerical and experimental validation
- Chapter 6 presents concluding remarks

Chapter 2

Dirty Derivatives Filter

2.1 Continuous-Time Dirty Filter

In this chapter, we consider a first-order approximate differentiator filter in continuous time domain. The filter dynamics are given by

$$\begin{aligned} \dot{q}_c(t) &= -a(q_c(t) + be(t)) \\ \vartheta(t) &= q_c(t) + be(t) \end{aligned} \tag{1}$$

Where:

- $q_c(t)$ is an auxiliary variable
- $e(t)$ is the error signal defined as $e(t) \triangleq y_d(t) - y(t)$
    - $y_d(t)$ denotes the desired reference output
    - $y(t)$ denotes the actual plant output
- The constants a and b are positive scalars
- $\vartheta(t)$ is the filter output

Since a is a strictly positive scalar, it follows that the system in (1) is Bounded-Input Bounded-Output (BIBO) stable.

The frequency magnitude response, given by

$$\left|\frac{\vartheta(j\omega)}{E(j\omega)}\right| = \frac{b\omega}{\sqrt{a^2+\omega^2}}$$

represents a high-pass filter with a cut-off frequency $\omega_c \cong a$. For operating frequencies $\omega < a$, this filter would approximate an ideal differentiator. In other terms, the bandwidth of the resulting ideal differentiator is not larger than a. As such, in the case where the range of operating frequencies is uncertain and in the absence of noise, it follows that larger values of a would result in more accurate approximations; that is, no upper bound on a would be imposed. Fig. 1 and Fig. 2 represent the magnitude and phase responses of the DF for $a = b = 1000$ and $a = b = 5000$, respectively.

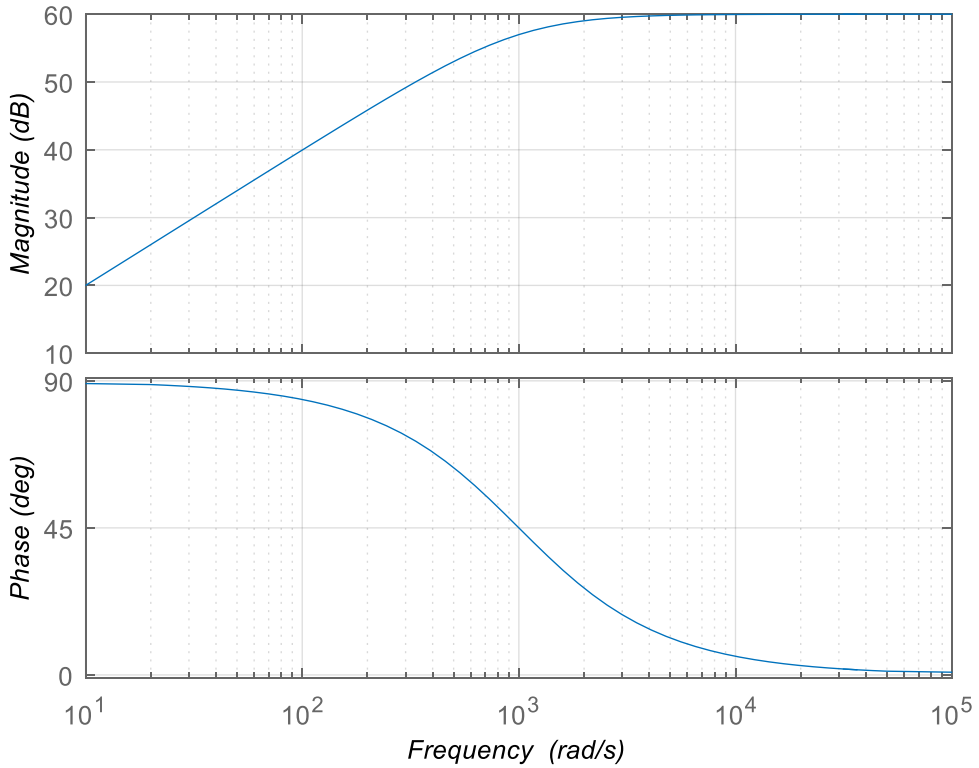

Figure 1. Magnitude and Phase response of the DF for $a = b = 1000$

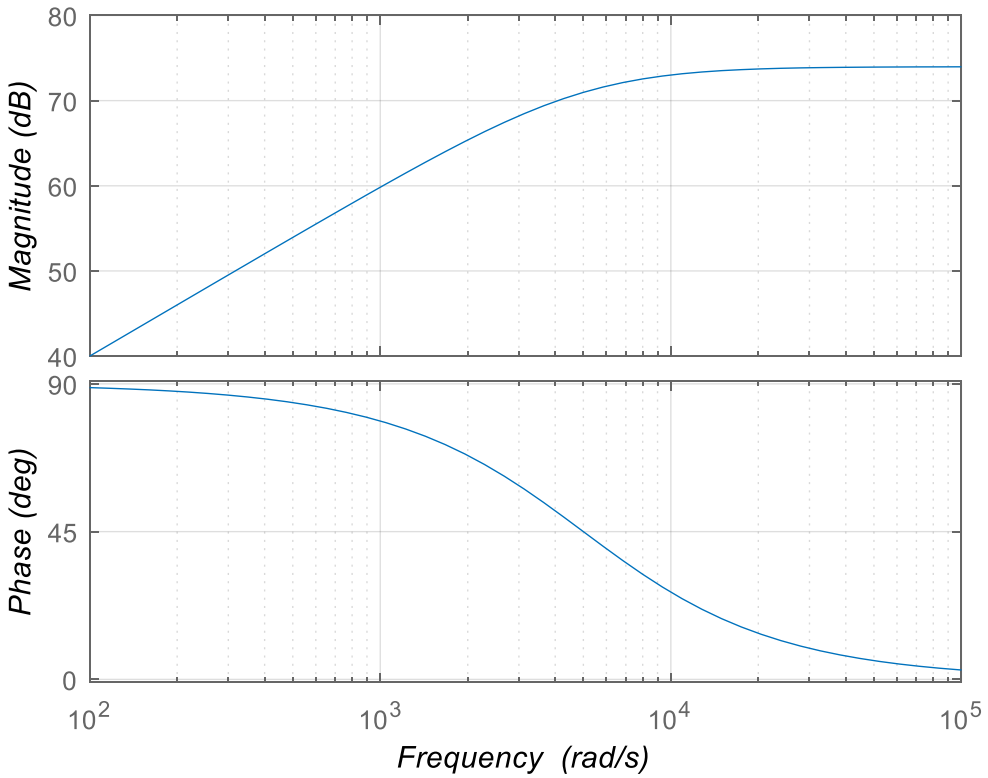

Figure 2. Magnitude and Phase response of the DF for $a = b = 5000$

In the following section, we demonstrate that the latter does not hold true in the *discrete-time* realization of this filter.

2.2 Discrete-Time Filter Performance

For real-time applications, we integrate $\dot{q}_c$ using a discretization method in order to obtain a difference equation similarly to the discretization of continuous-time state space systems, which is usually obtained by passing the discrete sequence of $e(k)$ through a zero-order hold. From (1), we can express $q_c(t)$ as follows

$$q_c(t) = \mathrm{e}^{-a(t-t_0)} q_c(t_0) + \int_{t_0}^{t} \mathrm{e}^{-a(t-\tau)} (-ab) e(\tau) d\tau$$

Let $t \equiv (k+1)T_s$ and $t_0 \equiv kT_s$, where k is the discrete-time index and T_s is the sampling period, then $q_c(t)$ can be further expressed as follows

$$q_c((k+1)T_s) = \mathrm{e}^{-aT_s} q_c(kT_s) + \int_{kT_s}^{(k+1)T_s} \mathrm{e}^{-a\left((k+1)T_s-\tau\right)} (-ab) e(\tau) d\tau$$

We assume that for all k and $kT_s \leq \tau \leq (k+1)T_s$

$$e(\tau) \cong e(kT_s)$$

As a result, $q_c(t)$ is now given by

$$q_c((k+1)T_s) \cong \mathrm{e}^{-aT_s} q_c(kT_s) - (ab) e(kT_s) \int_{kT_s}^{(k+1)T_s} \mathrm{e}^{-a\left((k+1)T_s-\tau\right)}\, d\tau$$

Let $\lambda = -((k+1)T_s - \tau)$ then $d\lambda = d\tau$ and

$$\int_{kT_s}^{(k+1)T_s} \mathrm{e}^{-a\left((k+1)T_s-\tau\right)}\, d\tau = \int_{-T_s}^{0} \mathrm{e}^{a\lambda}\, d\tau = \frac{1}{a}(1 - \mathrm{e}^{-aT_s})$$

Let $(k+1)T_s$ and kT_s be indexed by $k+1$ and k, respectively. As a result, the discrete-time Dirty Filter is given by

$$\begin{aligned} q_c(k+1) &= e^{-aT_s} q_c(k) + b(e^{-aT_s} - 1) e(k) \\ \vartheta(k) &= q_c(k) + be(k) \end{aligned} \tag{2}$$

The main objective of the filter is the estimation of the derivative of the error signal, $\dot{e}(k)$. In order to motivate the employment of this filter, we use a test signal

$$e(t) = e_o \sin(\omega_0 t) + \eta(t)$$

Where $\eta(t)$ is uniformly distributed zero-mean white noise.

We vary the operating frequency and the magnitude of the test signal $e(t)$ over the ranges $\omega_0 \in \{1,5,10,15,20,25\}$ and $e_o \in \{0.1,1,10\}$, respectively. The standard deviation of $\eta(t)$ is set to 0.001. We run the simulations for $t \in [0,5]$ and we

independently use two sampling periods, $T_s \in \{0.001,\ 0.002\}$ seconds. We vary the filter bandwidth or the value of a from 1 to 1000 and set $b = a$. To evaluate the filter performance in approximating the error signal $\dot{e}(t) = e_o\,\omega_0 \cos(\omega_0 t)$, we consider the corresponding absolute relative error, defined as

$$Relative\ Error \triangleq \frac{\underset{0.2\le t\le 5}{\text{avg}}\ |e_o\,\omega_0\cos(\omega_0 t) - \vartheta(t)|}{\underset{0.2\le t\le 5}{\text{avg}}\ |e_o\,\omega_0\cos(\omega_0 t)|}$$

The plots of relative errors for various values of a and for a sampling frequency $F_S = 1/T_S \in \{500,1000\}$ Hz are illustrated in Fig. 3, 4 and 5 for e_0 =0.1, 1 and 10, respectively.

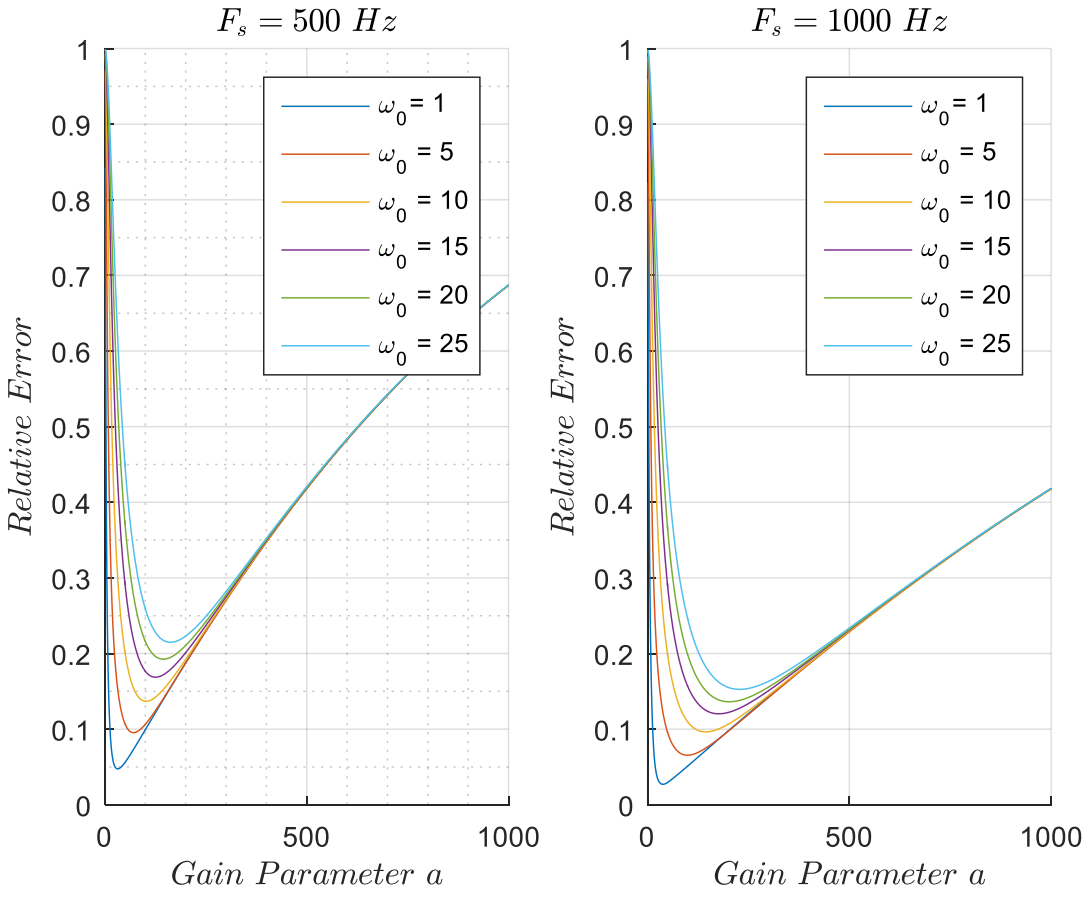

Figure 3. Plot of relative error vs. gain parameter a for $e_0 = 0.1$

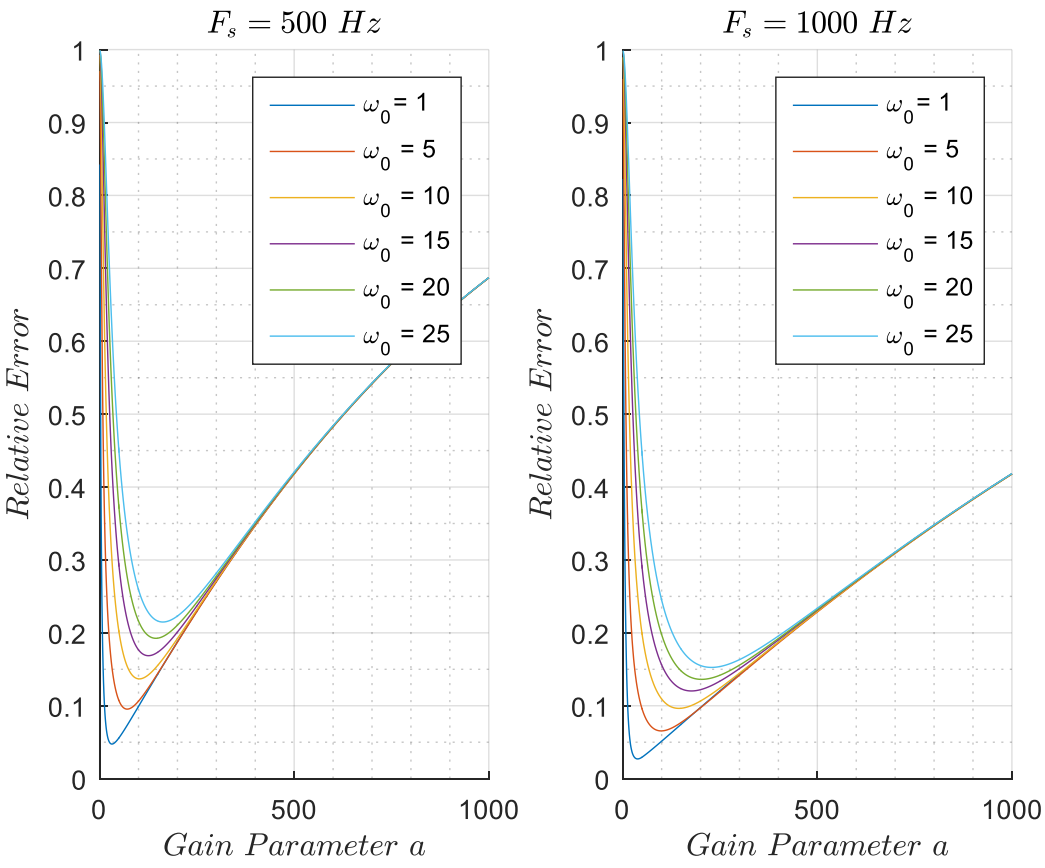

Figure 4. Plot of relative error vs. gain parameter a for $e_0 = 1$

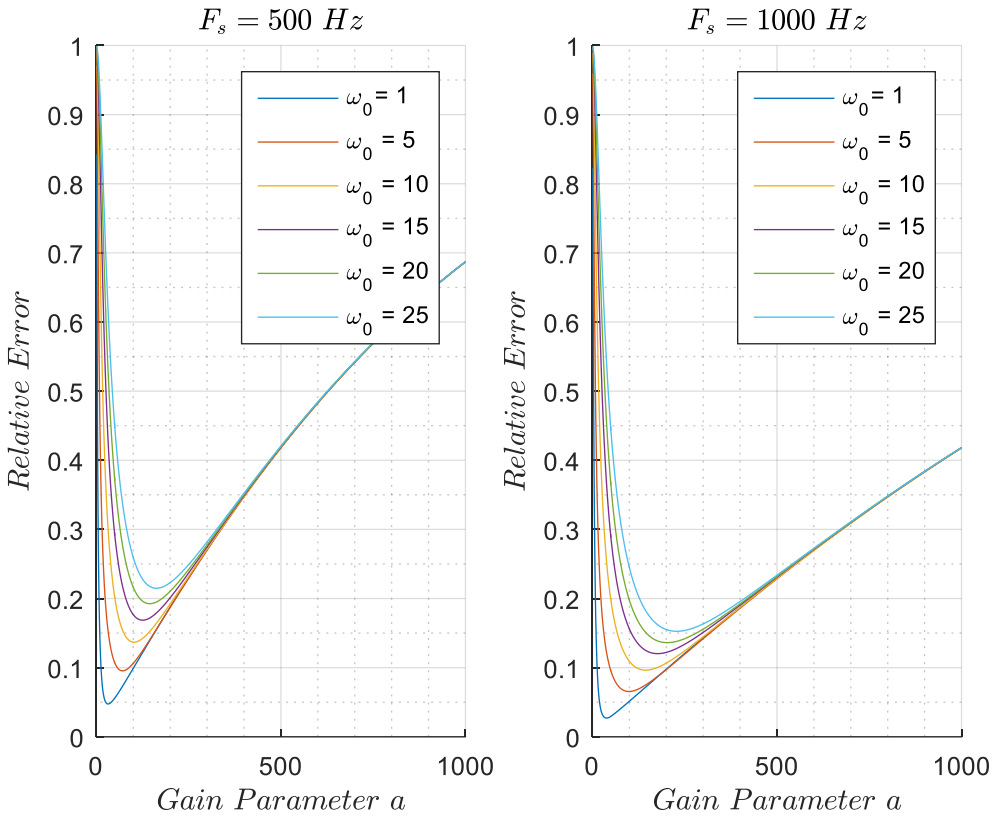

Figure 5. Plot of relative error vs. gain parameter a for $e_0 = 10$

The following conclusions are made:

- The value of a for which the filter achieves its best performance increases as ω_0 increases.
- The value of a is independent of the magnitude e_o, that is, relative errors remain the same for different $e_o \in \{0.1,1,10\}$.
- The values of a for which the filter achieves its best performance corresponding to $T_s = 0.001$ sec are about 40% larger than those corresponding to $T_s = 0.002$ sec.
- The minimum relative error values corresponding to $T_s = 0.002$ sec are about 40% larger than the ones corresponding to $T_s = 0.001$ sec.

Remark 1. In absence of noise, $\eta(t) = 0$, the improvement in performance turns out to be insignificant. However, if the standard deviation of the noise under consideration is increased by orders of magnitude, then the deterioration in performance becomes significant. □

Remark 2. Other discretization methods were also simulated such as linear interpolation of inputs, bilinear (Tustin) approximation, matched pole-zero method, Euler, and least-squares minimization of the error between frequency responses of the continuous and discrete systems. The results obtained using these methods yielded the same properties as the one employed in (2). □

The latter results suggest that the value of the parameter a that yields best performance varies as the frequency of the input signal varies. In other terms, for the cases where the operating frequency varies, one must subsequently vary the bandwidth of the filter in order to preserve its optimal performance. One class of such a filter is proposed in Chapter 4.

2.3 Discrete-Time Filter Characteristics

Consider the system in (2) and let $\xi(.)$ represent measurement error, then

$$\hat{e}(k) = e(k) + \xi(k) = y_d(k) - y(k) + \xi(k) \tag{3}$$

Assumptions:

(A1) The measurement error $\xi(k)$ is bounded $\forall\ k \geq 0$.

(A2) $BW_e < a \ll \frac{1}{T_s}$, where BW_e denotes the bandwidth of $e(k) = y_d(k) - y(k)$.

In all the results that follow, we assume that (A1) and (A2) hold.

Proposition 1: **There exists a bounded sequence $\boldsymbol{\gamma(k)}$, such that**

$$\boldsymbol{\vartheta(k+1) = e^{-aT_s}\vartheta(k) + T_s b(\dot{e}(k) + \gamma(k))} \quad \textbf{(4)}$$

Proof of Proposition 1:

From (2), we have

$$q_c(k+1) = e^{-aT_s}q_c(k) + b(e^{-aT_s} - 1)\hat{e}(k)$$

or

$$q_c(k+1) - q_c(k) = (e^{-aT_s} - 1)q_c(k) + b(e^{-aT_s} - 1)\hat{e}(k)$$

As a result, we have

$$\vartheta(k+1) - \vartheta(k) = q_c(k+1) - q_c(k) + b(\hat{e}(k+1) - \hat{e}(k))$$

or equivalently,

$$\vartheta(k+1) - \vartheta(k) = (e^{-aT_s} - 1)q_c(k) + b(e^{-aT_s} - 1)\hat{e}(k) + b\big(\hat{e}(k+1) - \hat{e}(k)\big)$$

Substituting $\vartheta(k) = q_c(k) + b\hat{e}(k)$ into the latter, we get

$$\vartheta(k+1) = q_c(k) + b\hat{e}(k) + (e^{-aT_s} - 1)q_c(k)$$

$$+b(e^{-aT_s} - 1)\hat{e}(k) + b(\hat{e}(k+1) - \hat{e}(k))$$

Expanding and collecting terms, we obtain

$$\vartheta(k+1) = e^{-aT_s}\vartheta(k) + b(\hat{e}(k+1) - \hat{e}(k)) \quad (5)$$

Consider $\delta\hat{e}(k) \triangleq \hat{e}(k+1) - \hat{e}(k)$. Thus,

$$\delta\hat{e}(k) = e(k+1) - e(k) + \delta\xi(k)$$

Where $\delta\xi(k) \triangleq \xi(k+1) - \xi(k)$.

With (A2), we can approximate $\dot{e}(k)$ as

$$\dot{e}(k) \cong \frac{e(k+1) - e(k)}{T_s}$$

Since $\xi(k)$ is always bounded, then

$$\gamma(k) \triangleq \frac{\xi(k+1) - \xi(k)}{T_s}$$

is bounded for all k.

To this end, (5) can be written as

$$\vartheta(k+1) = e^{-aT_s}\vartheta(k) + T_s b(\dot{e}(k) + \gamma(k)) \square$$

If $aT_s \ll 1$, then

$$\vartheta(k+1) \cong (1 - aT_s)\vartheta(k) + T_s b(\dot{e}(k) + \gamma(k))$$

The equation above represents a first-order infinite impulse response low-pass filter. In addition, whenever $a = b$, this filter is also known as an exponentially weighted moving average [57], where the weighting for each older datum decreases exponentially. The coefficient $T_s a$ represents a smoothing factor. Higher values of $T_s a$ cause a faster decrease in the weightings of older datums or increases the smoothing effect.

It follows that although the input to the filter is the error signal $\boldsymbol{e(k)}$, the filter output is a *smooth* version of the signal $\{\dot{\boldsymbol{e}}(\boldsymbol{k}) + \boldsymbol{\gamma}(\boldsymbol{k})\}$

It should be noted that due to the inherited low-pass nature of system (4), the high frequencies of $\gamma(k)$ are significantly attenuated [58].

Theorem 1: **With $\boldsymbol{\gamma(k) \cong 0}$, there exists a positive bounded constant $\boldsymbol{\kappa}$ such that $\forall\ \boldsymbol{k > \kappa}$, we have**

$$\boldsymbol{\vartheta_{a \neq b}(k) \cong \frac{b}{a}\vartheta_{b=a}(k)} \quad \textbf{(6)}$$

Proof of Theorem 1:

In the following, we conduct the analysis for two different cases:

- $a = b$
- $a \neq b$

Case 1: $\boldsymbol{a = b}$

For $aT_s \ll 1$ and $\gamma(k) \cong 0$, (4) can be further expressed as

$$\vartheta_{b=a}(k+1) \cong (1 - aT_s)\vartheta_{b=a}(k) + aT_s\dot{e}(k)$$

Let $\lambda = 1 - aT_s$, then (4) is given by

$$\vartheta_{b=a}(k+1) \cong \lambda\vartheta(k) + (1-\lambda)\dot{e}(k)$$

Iterating the latter equation, we get

$$\vartheta_{b=a}(k) \cong \lambda^k\vartheta_{b=a}(0) + (1-\lambda)\sum_{i=0}^{k-1}\lambda^{k-i-1}\dot{e}(i) \quad (7)$$

As indicated, (7) represents an exponentially weighted moving average with a smoothing factor of $1 - \lambda < 1$. As a result, there exists a positive constant κ such that $\forall\ k > \kappa$

$$\lambda^k\vartheta_{b=a}(0) \cong 0$$

thus

$$\vartheta_{b=a}(k) \cong (1-\lambda)\sum_{i=0}^{k-1}\lambda^{k-i-1}\dot{e}(i) \quad (8)$$

Case 2: $a \neq b$

For $aT_s \ll 1$ and $\gamma(k) \cong 0$, (4) can be further expressed as

$$\vartheta_{a\neq b}(k+1) \cong \lambda\vartheta_{a\neq b}(k) + \frac{b}{a}(1-\lambda)\dot{e}(k)$$

Iterating the latter equation, we get

$$\vartheta_{a\neq b}(k) \cong \lambda^k\vartheta_{a\neq b}(0) + \frac{b}{a}(1-\lambda)\sum_{i=0}^{k-1}\lambda^{k-i-1}\dot{e}(k) \quad (9)$$

Similarly, $\forall\, k > \kappa$, (9) can be approximated by

$$\vartheta_{a\neq b}(k) \cong \frac{b}{a}(1-\lambda)\sum_{i=0}^{k-1}\lambda^{k-i-1}u(i) \quad (10)$$

Equations (8) and (10) imply that imply that $\forall\, k > \kappa$,

$$\vartheta_{a\neq b}(k) \cong \frac{b}{a}\vartheta_{b=a}(k) \qquad \square$$

Theorem 1 neglects $\gamma(k)$, which accounts for output measurement errors. In addition, for $k \leq \kappa$, equations (8) and (10) also neglect the transient $\lambda^k\vartheta(0)$. As such, equation (6) can be further extended to accommodate the latter, such that

$$\vartheta(k) = \frac{b}{a}\dot{e}(k) + \upsilon(k) \quad (11)$$

Where $\upsilon(k)$ is a bounded sequence.

In the following chapter, we integrate filter (2) with a conventional SMC. Subsequently, we present stability analysis of the closed-loop control.

Although the literature is swamped with variations of SMC controllers, we resort to the conventional SMC for the fact that it highly suffers from the chattering phenomena. We aim to show how the smoothing characteristics of the DF can significantly reduce the chattering in SMC while preserving a good tracking performance.

Chapter 3

Stability Analysis

3.1 Non-Linear Robot Dynamics

We consider the Euler-Lagrange model describing the continuous-time dynamics of rigid n-link serial non-redundant robot manipulator, with all actuated revolute joints, which is given by

$$\tau = M(q)\ddot{q} + C(q,\dot{q})\dot{q} + G(q) + F(q,\dot{q}) \tag{12}$$

Where:

- $q, \dot{q},$ and $\ddot{q} \in \mathbb{R}^n$ represent joint angles, velocities and accelerations respectively
- $M(q) \in \mathbb{R}^{n\times n}$ is the symmetric positive definite inertia matrix
- $C(q,\dot{q}) \in \mathbb{R}^{n\times n}$ denotes the Coriolis and centripetal matrix
- $G(q) \in \mathbb{R}^n$ is the gravity vector
- $F(q,\dot{q}) \in \mathbb{R}^n$ represents the joint friction
- $\tau \in \mathbb{R}^n$ denotes the joint torque input.

We now present some structural properties [58] of (11):

(S1) There exists positive scalars ϱ_1 and ϱ_2 such that

$$0 < \varrho_1 < \mathbb{E}_m\big(M(q)\big) \leq \mathbb{F}\big(M(q)\big) \leq \mathbb{E}_M\big(M(q)\big) < \varrho_2 < \infty$$

Where:

- $\mathbb{E}_m\big(M(q)\big)$ is the minimum eigenvalue of M
- $\mathbb{E}_M\big(M(q)\big)$ is the maximum eigenvalue of M
- $\mathbb{F}\big(M(q)\big)$ is the induced Forbenius norm

As previously mentioned, $M(q)$ is a symmetric positive definite matrix. As a result, structural property (S1) implies the following:

(S2) There exists positive scalars ϱ_3 and ϱ_4 such that

$$0 < \varrho_3 < \mathbb{E}_m\big(M^{-1}(q)\big) \leq \mathbb{F}\big(M^{-1}(q)\big) \leq \mathbb{E}_M\big(M^{-1}(q)\big) < \varrho_4 < \infty$$

(S3) There exists a positive scalar ϱ_5 such that

$$\|g(q)\| \leq \varrho_5 < \infty$$

Where $\|\cdot\|$ is the Euclidean norm

3.2 Proposed SMC Scheme

We can express (12) as

$$\ddot{q} = M^{-1}(q)\tau - M^{-1}(q)G(q) - M^{-1}(q)\big(C(q,\dot{q})\dot{q} + F(q,\dot{q})\big)$$

Next, we write an expression for $\ddot{e} \triangleq \ddot{q}_d - \ddot{q}$ as follows

$$\ddot{e} = \ddot{q}_d - M^{-1}(q)\tau + M^{-1}(q)G(q) + M^{-1}(q)\big(C(q,\dot{q})\dot{q} + F(q,\dot{q})\big) \qquad (13)$$

The proposed SMC scheme is given by

$$\tau = G(q) + C(q,\dot{q})\dot{q} + M(q)\big(\ddot{q}_d + \Lambda K_{DF}^{-1}\vartheta + \mathrm{Ksgn}(s)\big) \qquad (14)$$

Where:

- $K \in \mathbb{R}^{n\times n}$ and $\Lambda \in \mathbb{R}^{n\times n}$ are diagonal positive gain matrices
- $K_{DF} \in \mathbb{R}^{n\times n}$ is a diagonal matrix with the i^{th} diagonal entry being b_i/a_i of (11)
- *T*he elements of ϑ are the outputs of the adaptive approximate differentiator filter associated with each joint
- $s \in \mathbb{R}^n$ is the sliding variable given by

$$s = K_{DF}^{-1}\vartheta + \Lambda e \tag{15}$$

In the next section, we provide a stability analysis of the proposed scheme (14). We use the continuous-time domain in our subsequent analysis for simplicity.

3.3 Stability Analysis

***Theorem* 2. For sufficiently large K and Λ, the SMC in (14) and (15) is stable in the sense of Lyapunov.**

Proof of Theorem 2. According to (11), there exists a bounded sequence, v_i for $i \in \{1,..,n\}$, such that

$$\vartheta_i \cong \frac{b_i}{a_i}\dot{e}_i + v_i$$

Therefore, $K_{DF}^{-1}\vartheta$ can be expressed as

$$K_{DF}^{-1}\vartheta \cong \dot{e} + \bar{v}$$

Where:

- The elements of the diagonal matrix K_{DF} are equal to b_i/a_i
- $\bar{v}_i = \frac{a_i}{b_i}\, v_i$ is bounded

Consequently, (14) can be further expressed as

$$\tau = G(q) + C(q,\dot{q})\dot{q} + M(q)(\ddot{q}_d + \Lambda\dot{e} + \mathrm{Ksgn}(s) + \Lambda\bar{v}) \tag{16}$$

And (15) becomes

$$s = \dot{e} + \Lambda e + \bar{v} \tag{17}$$

We define $\bar{s} \triangleq \dot{e} + \Lambda e$ and select the Lyapunov function

$$V = \frac{1}{2}\bar{s}^T\bar{s}$$

Therefore,

$$\dot{V} = \bar{s}^T\dot{\bar{s}} = \bar{s}^T(\ddot{e} + \Lambda\dot{e}) \tag{18}$$

Inserting (16) in (13), we obtain

$$\ddot{e} = -\mathrm{Ksgn}(s) - \Lambda\dot{e} + Y \tag{19}$$

where $Y = M^{-1}(q)F(q,\dot{q}) - \Lambda\bar{v}$.

Given the fact that both $M^{-1}(q)F(q,\dot{q})$ (see, e.g., [58] [56]) and $\bar{v}$ are bounded, it follows that Y is also bounded.

Inserting (19) in (18), we obtain

$$\dot{V} = \bar{s}^T(-\mathrm{Ksgn}(s) + Y)$$

If the position error, e is zero, then convergence is achieved. Otherwise, since Λ is a positive definite matrix, despite the size of $\bar{v}$, we can choose Λ large enough such that

$$\mathrm{sgn}(s) = \mathrm{sgn}(\bar{s})$$

Where:

- $s = \dot{e} + \Lambda e + \bar{v}$

- $\bar{s} = \dot{e} + \Lambda e$

The argument can be thought of while considering each joint separately. Of note, as presented in the proof of (4), the exponentially weighted moving average nature of the DF makes the amplitude of $\bar{v}$ very small whenever the measurement errors of the joint angle, ξ, are relatively small, which is the case in practical applications.

Thus, for sufficiently large Λ, we obtain

$$\dot{V} = \bar{s}^T Y - \sum_{i=1}^{n} \beta_i |\bar{s}_i|$$

Where:

- $\bar{s}_i$ represents the i^{th} element of $\bar{s}$
- β_i represents the i^{th} diagonal entry of the controller gain K

If $\bar{s} = \dot{e} + \Lambda e$ is zero then $e(t) = \exp(-\Lambda t)\, e(0)$, which is stable since $\Lambda > 0$, and the Lyapunov function, $V = \frac{1}{2}\bar{s}^T\bar{s}$, becomes zero or reaches its ideal minimum.

Otherwise and since the system $\dot{e} + \Lambda e \neq 0$ is stable ($\Lambda > 0$), and Y is always bounded, we choose sufficiently large values of β_i such that $\dot{V} < 0$. The latter satisfies the Lyapunov stability criterion. □

Chapter 4

Proposed Filter

4.1 Approximate Differentiator with Varying Bandwidth

As previously indicated, the value of the filter bandwidth, a, that yields optimal filter performance varies with the bandwidth of the input signal. In the position tracking problem of robot manipulators, the bandwidth of the position signal can be significantly larger than the bandwidth of the reference trajectory. In case of sound output tracking, the magnitude of the position error signal becomes relatively small as the position output signal approaches its corresponding reference trajectory and consequently, the bandwidth of the position signal would be close to that of the reference signal. Whenever an adequate controller is designed, one can expect that the output errors are mostly due to chaotic friction forces and/or poor estimation of the joint velocity errors, $\dot{e}(.)$. Accordingly, one can suspect that the magnitude of the position error signal and the variations of the signal bandwidth beyond the bandwidth of the reference trajectories are correlated. Consequently, by letting the value of a depend on the magnitude of the output position error, the bandwidth of the filter will

consequently vary to yield a better estimation of the velocity error signal, $\dot{e}(.)$, as the bandwidth of the output position signal itself varies.

Inspired by the latter, we propose the following adaptation law for the two filter parameters a and b of the approximate differentiator filter, corresponding to the i^{th} joint:

$$\begin{aligned} a_i(k) &= \min(a_i^r + a_i^e|e_i(k)|, \tfrac{1}{2T_s}) \\ b_i(k) &= \alpha_i a_i(k) \end{aligned} \tag{20}$$

Where:

- $0 < a_i^r \ll \frac{1}{2T_s}$ is selected based on the bandwidth of its corresponding reference tracking trajectory signal
- $\alpha_i \geq 1$ is a scaling parameter
- a_i^e is an error scaling parameter that can be easily selected while tuning the closed-loop system

In the case where $|e_i(k)|$ is very large at any time instant such that $a_i^r + a_i^e|e_i(k)| > \frac{1}{2T_s}$, then $a_i(k)$ is limited to $\frac{1}{2T_s}$. The latter bound is selected based on (A2) and the filter performance; see, e.g., Fig. 3, 4 and 5.

In what follows, we will refer to the filter in (2) under the adaptation law (20) as the Approximate Differentiator with Varying Bandwidth (ADVB).

Chapter 5

Performance Evaluation

5.1 Barret Whole-Arm-Manipulator Description

The evaluations are conducted on a 4-DOF Barret WAM, shown in Fig. 6, with a reach of 1m and a payload of 4 kg.

Figure 6. Barret WAM [59]

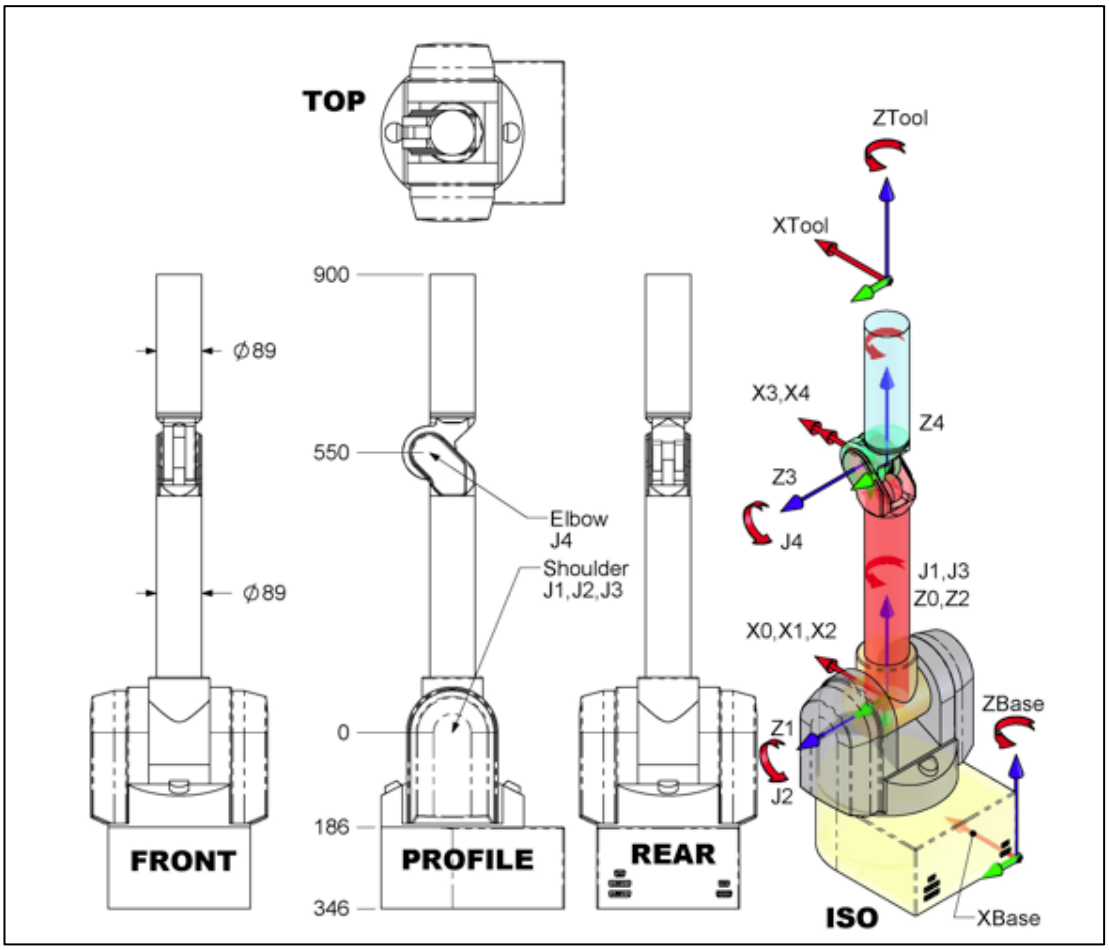

Figure 7. 4 - DoF WAM Joints and Frames [60]

The 4 DoF WAM has 4 joints (J1 - J4) that are cable-driven, along with 4 brushless DC motors (M1 - M4). Motor 1, located at the base of the manipulator, controls the yaw (J1). Motors 2 and 3, located in the WAM shoulder, control the pitch (J2) and roll (J3). Motor 4 controls the elbow of the manipulator and is also located in the WAM shoulder. The entire configuration is detailed in Fig. 7. Near each motor is a compact package containing 12-bits position encoders, controllers and power amplifiers. Every joint is mechanically limited in motion. The joint limits, as per the axes depicted in Fig. 7, are listed in Table I.

Table I. Barret WAM Joint Limits (Deg) [60]

Joint	Positive Joint Limit (Deg)	Negative Joint Limit (Deg)
J1	150	-150
J2	113	-113
J3	157	-157
J4	180	-50

For the experimental evaluations, the Barret WAM is operated using MATLAB SIMULINK. It is connected to a host PC with core i5, through an external target PC, which in turn is connected to the robotic arm through Barret CAN bus. The target PC is a core i7 and is booted using a MATLAB kernel. For the numerical simulations, the employed WAM model along with the friction model are fully described in [30]. Based on the joint position Barrett WAM sensor specifications, we add zero-mean uniformly distributed measurement noise bounded by $\pm 10^{-4}$ or with a variance of $4 \times 10^{-8}/12$ to the joint position measurements.

5.2 Description of Conducted Simulations

In the first example, we numerically simulate the performance of a conventional SMC while employing the Approximate Differentiator (DF) (2) and a High-Gain Observer (HGO). The simulation employs *sinusoidal* trajectories. The comparison is based on the resulting tracking error for all joints as well as the smoothness of the torques. This example further illustrates the importance of the smoothing characteristics of the DF.

In the second example, we numerically simulate the performance of a conventional SMC while employing the DF (2) and the proposed ADVB (19). In this simulation, we employ *parabolic* trajectories. This example shows how the ADVB consistently improves the tracking performance of the SMC when compared to DF.

In the third example, we experimentally integrate the DF with a conventional SMC. We illustrate the convex trend in the performance of the DF by varying its bandwidth and consequently identifying an "optimal" DF. Next, we integrate the proposed ADVB with a conventional SMC and show how it consistently improves the tracking performance when compared to the "optimal" DF, and for different employed parameters.

We resort to two sets of reference trajectories defined over $t \in [0,5]$ sec. The sinusoidal reference trajectories are defined as follows:

$$\begin{cases} q_{i,d}(t) = \frac{\pi}{3}\left(1 - \cos\left(\frac{\pi}{2}t\right)\right) + \hat{q}_{i,d}(0), i \in \{1,2\} \\ q_{3,d}(t) = \frac{\pi}{3}(1 - \cos(\pi t)) + \hat{q}_{3,d}(0) \\ q_{4,d}(t) = -\frac{\pi}{3}\left(1 - \cos\left(\frac{\pi}{2}t\right)\right) + \hat{q}_{4,d}(0) \end{cases}$$

Similarly, the parabolic reference trajectories are given by:

$$\begin{cases} q_{1,d}(t) = \frac{1}{8}t^2 + \hat{q}_{1,d}(0) \\ q_{2,d}(t) = \frac{1}{8}t^2 + \hat{q}_{2,d}(0) \\ q_{3,d}(t) = \frac{1}{4}t^2 + \hat{q}_{3,d}(0) \\ q_{4,d}(t) = -\frac{1}{8}t^2 + \hat{q}_{4,d}(0) \end{cases}$$

Where $\hat{q}_{i,d}(0), i \in \{1,..,4\}$ denotes an estimate of the arm home position. We denote $q_d = \left[q_{1,d} \dots q_{4,d}\right]^T$.

Throughout this work, we use the Mean Average Error (MAE) as a performance metric for the i^{th} joint, given by

$$MAE_i \triangleq \text{AVG}_{t\in[0,5]}\left|q_i - q_{d,i}\right|$$

In order to reduce the chattering effects in the SMC torque signals, we resort to the Boundary Layer (BL) approach [61] and replace the $sign$ function by the saturation function $\psi \in \mathbb{R}^n$ whose elements ψ_i are defined as

$$\psi_i = \frac{s_i}{|s_i| + \rho} \cong sgn(s)$$

where $0 < \rho \ll 1$ represents the width of the BL.

As a result, the SMC controller (14) becomes as follows

$$\tau = G(q) + M(q)(\ddot{q}_d + \Lambda K_{DF}^{-1}\vartheta + \text{K}\psi) \tag{21}$$

All evaluations use a sampling rate of 500 Hz.

5.3 Example 1

5.3.1 High-Gain Observer

In this section, we evaluate the tracking performance of a conventional SMC while using a DF and a HGO [62], where the latter is given by

$$\dot{\hat{x}}_1 = \hat{x}_2 + \frac{2}{\epsilon}(q - \hat{x}_1)$$

$$\dot{\hat{x}}_2 = \frac{1}{\epsilon^2}(q - \hat{x}_1) \tag{22}$$

Where:

- $\hat{x}_1, \hat{x}_2 \in \mathbb{R}^n$ correspond to the observed joint angles and velocities respectively
- $\epsilon \in \mathbb{R}$ relates to the observer gain

As previously reported in section 2.1, and in order to illustrate the estimation performance of this observer, we use a sinusoidal test signal

$$e(t) = e_o \sin(\omega_0 t) + \eta(t)$$

and we evaluate the absolute relative error for different sampling frequencies. We vary the operating frequency and the magnitude of the test signal $e(t)$ over the ranges $\omega_0 \in \{1,5,10,15,20,25\}$ and $e_o \in \{0.1,1,10\}$, respectively. The observer parameter ϵ is varied between 0.01 and 0.1 and the standard deviation of the uniformly distributed zero-mean white noise $\eta(t)$ is set to 0.001.The plots of relative errors for various values of ϵ and for a sampling frequency $F_S = 1/T_S \in \{500,1000\}$ Hz are illustrated in Fig. 8, 9 and 10.

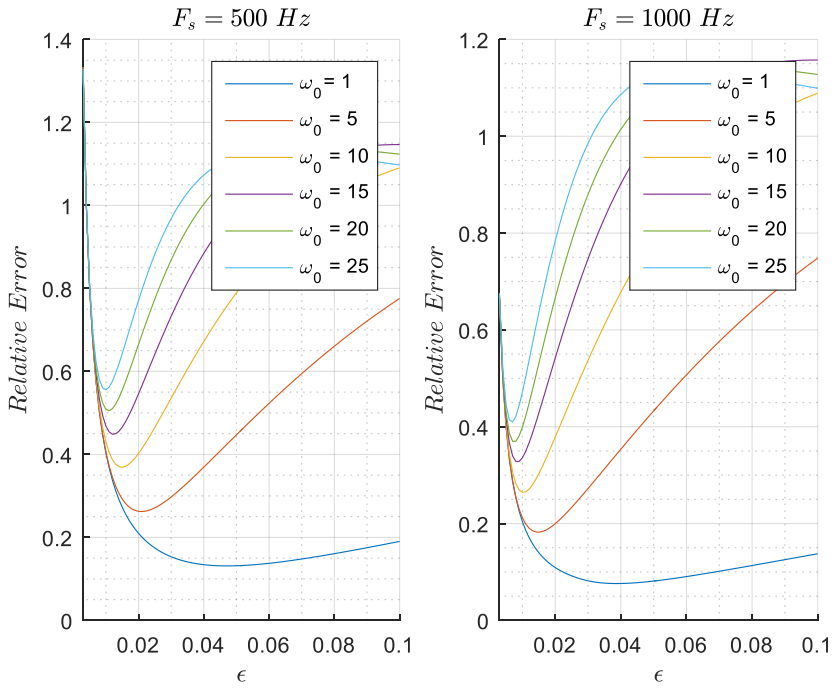

Figure 8. Plot of relative error vs. gain parameter ϵ for $e_0 = 0.1$

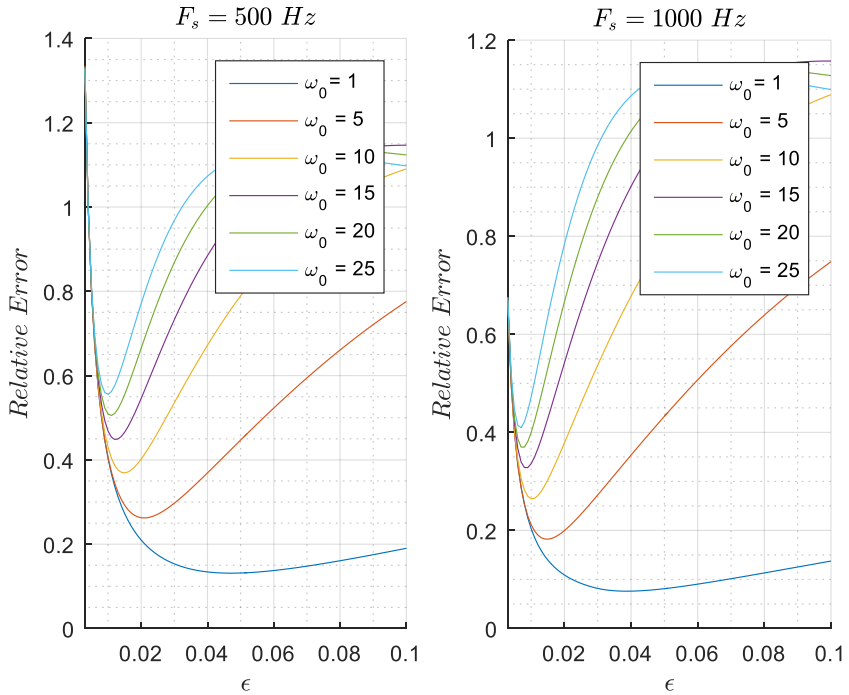

Figure 9. Plot of relative error vs. gain parameter ϵ for $e_0 = 1$

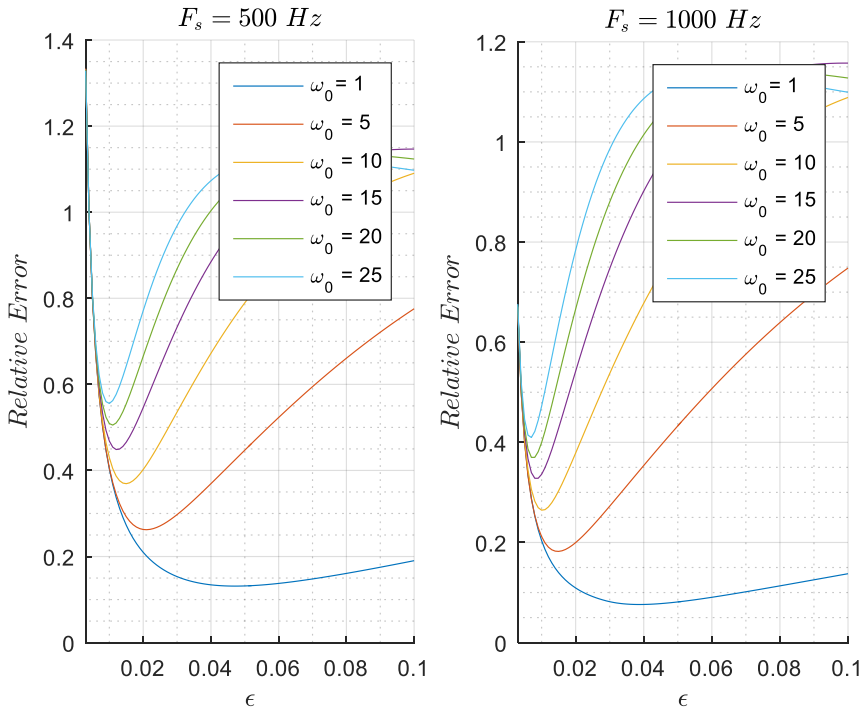

Figure 10. Plot of relative error vs. gain parameter ϵ for $e_0 = 10$

The following conclusions are made:

- The value of ϵ for which the filter achieves its best performance decreases as ω_0 increases.
- The value of ϵ is independent of the magnitude e_o, that is, relative errors remain the same for different $e_o \in \{0.1,1,10\}$.
- The values of ϵ for which the filter achieves its best performance corresponding to $T_s = 0.002$ sec are about 40% larger than those corresponding to $T_s = 0.001$ sec.
- The minimum relative error values corresponding to $T_s = 0.002$ sec are about 40% larger than the ones corresponding to $T_s = 0.001$ sec.

5.3.2 Numerical Results

In this section, we evaluate the tracking performance of a conventional SMC while employing the DF and then the HGO. For SMC, we set $\mathrm{K} = \mathrm{diag}(1,1,2,2)$, $\Lambda = 50\mathrm{K}$ and $\rho = 0.02$.

In order to examine the performance of the DF and the HGO as their parameters are varied, we numerically evaluate the average of the absolute error across all joints while varying the parameters a and ϵ, respectively. The results are illustrated in Fig. 11.

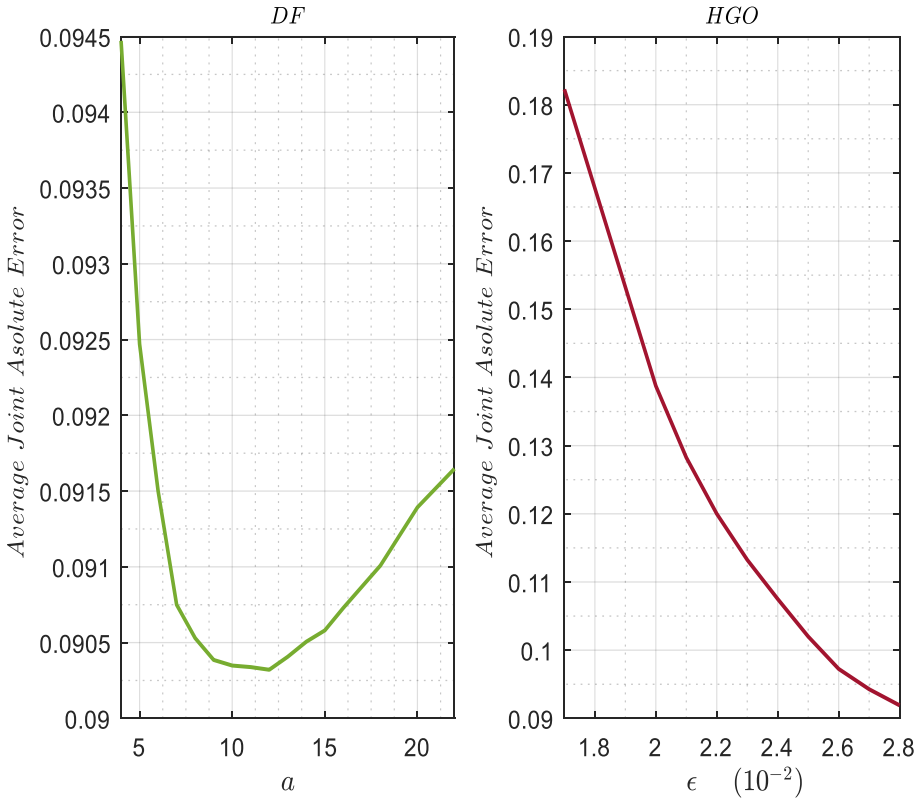

Figure 11. Average Joint Absolute Error using DF and HGO as a function of a and ϵ

As expected, the DF performance follows a *convex trend* as the filter bandwidth a is varied. For the HGO, we notice that as the parameter ϵ is increased from 0.017 to 0.028, the average joint absolute error constantly decreases.

Next, we integrate the DF and HGO with a conventional SMC and examine the tracking performance as well as the smoothness of the torque signals. For the HGO, we consider two cases where $\epsilon = 0.017$ and $\epsilon = 0.023$, respectively. Increasing the value of ϵ beyond $\epsilon = 0.023$ results in excessively large oscillations in the torque signals as elaborated in our subsequent demonstration. For the sake of comparison, we set the DF parameters, $a_i = b_i = 10$, for $i \in \{1,..,4\}$. The corresponding torque signals are illustrated in Fig. 12 and Fig. 13 whereas the tracking performance is reported in Table II.

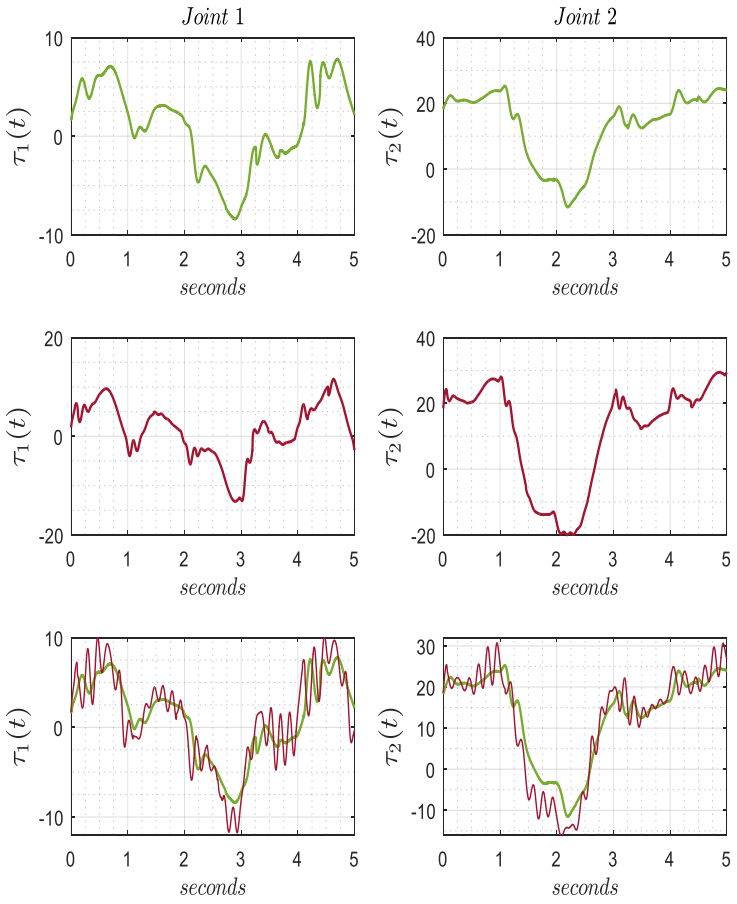

Figure 12. Plots of Joint Torques (1 and 2) for SMC Integrated with: DF (First Row) for $a = b = 10$, HGO (Second Row) for $\epsilon = 0.017$. The Third Row shows the torques of the DF (Green) for $a = b = 10$, and of the HGO (Red) for $\epsilon = 0.028$

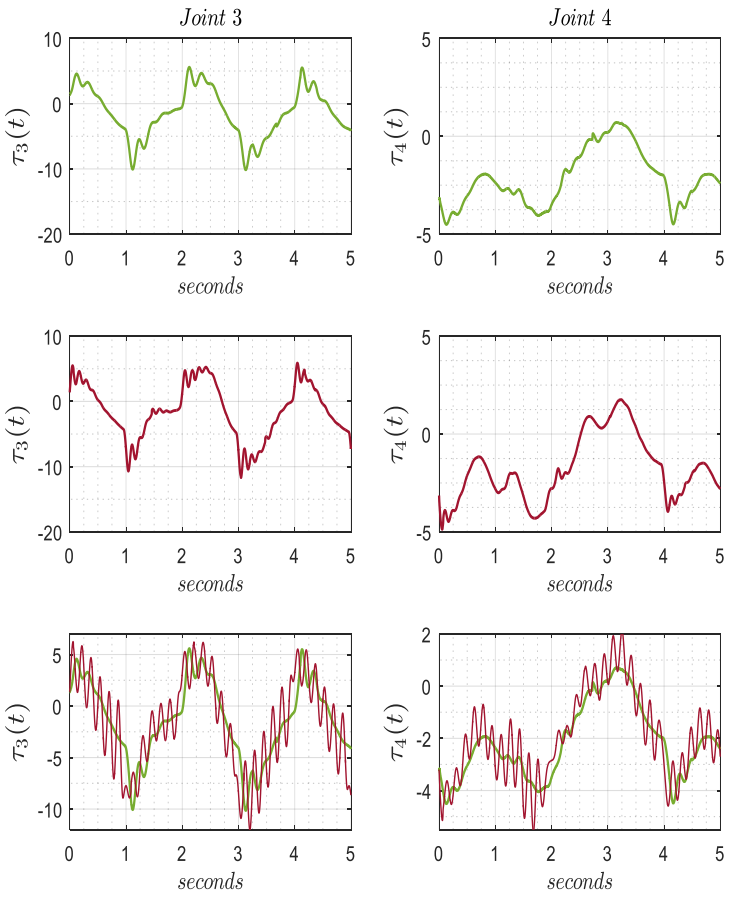

Figure 13. Plots of Joint Torques (3 and 4) for SMC Integrated with: DF (First Row) for $a = b = 10$, HGO (Second Row) for $\epsilon = 0.017$. The Third Row shows the torques of the DF (Green) for $a = b = 10$, and of the HGO (Red) for $\epsilon = 0.028$

Table II. MAE of all Joints for DF and HGO (Example 1)

Scheme	Joint 1	Joint 2	Joint 3	Joint 4	**Average**
DF $(a_i = 10)$	0.077	0.064	0.131	0.088	**0.090**
HGO $(\epsilon = 0.017)$	0.128	0.152	0.159	0.290	**0.182**
HGO $(\epsilon = 0.023)$	0.068	0.094	0.116	0.175	**0.113**

By examining the results of Table II, Fig. 11, Fig. 12 and Fig. 13, we conclude the following:

- As ϵ is increased from 0.017 to 0.028, the tracking performance while employing the HGO increases as the torques start to exhibit strong oscillations. In particular, the oscillations resulting from the HGO in Fig. 3, for $\epsilon = 0.028$, that lead to undesired arm vibrations. It should be noted that, especially for a conventional SMC, non-smooth velocity estimations could cause joint torque saturations. The smoothness of the actual torques is critical to avoid such issues and to guarantee the safety of the setup. In fact, the resulting torques while employing the HGO start to exhibit significant vibrations at $\epsilon = 0.023$, which explains our choice of parameters in Table I. For $\epsilon = 0.017$, the resulting torques of the HGO are almost as smooth as the ones resulting from using the DF at $a_i = 10$.

- On average, and while keeping the torques smooth enough, the resulting joint tracking absolute errors corresponding to DF are 20 % to 50 % lower than the ones obtained when employing the HGO.
- The same performance provided by the HGO can be obtained by the DF but with much smoother torques. This further illustrates the importance of the smoothing characteristics of the DF, especially in applications where velocity estimation is critical.

Remark 3. For SMC, joint velocity can also be estimated using Euler differentiation or Kalman filtering, however:

- Euler Differentiation result in very large oscillations in torque signals.
- For Kalman Filtering, both DF and HGO achieved a significantly higher tracking performance when integrated with SMC. □

5.4 Example 2

Using parabolic reference trajectories, we compare the tracking performance of a conventional SMC while employing the DF and the proposed ADVB. The aim is to show how the ADVB decreases the tracking errors beyond the capabilities of the DF. To do so, we begin by integrating the DF with a conventional SMC. We vary the filter bandwidth and record the average tracking performance across all joints for $a_i \equiv b_i = a$. By doing so, we identify the value of a that achieves the best tracking performance of the SMC. Next, we integrate the ADVB with the conventional SMC and report the resulting tracking errors. Table III lists the MAE of all joints for all the conducted simulations. Fig. 14 and Fig. 15 plot the resulting joint angles and joint torques, respectively, for both schemes under consideration.

Table III. MAE of all Joints for DF and ADVB (Example 2)

Scheme	Joint 1	Joint 2	Joint 3	Joint 4	**Average**
DF $a_i = 11$	0.0560	0.0441	0.1557	0.0583	**0.0785**
ADVB $a_i^r \equiv b_i^r = a^r = 2$ $a_1^e = 50, a_2^e = 100$ $a_3^e = 50, a_4^e = 100$	0.0442	0.0334	0.1073	0.0419	**0.0567**

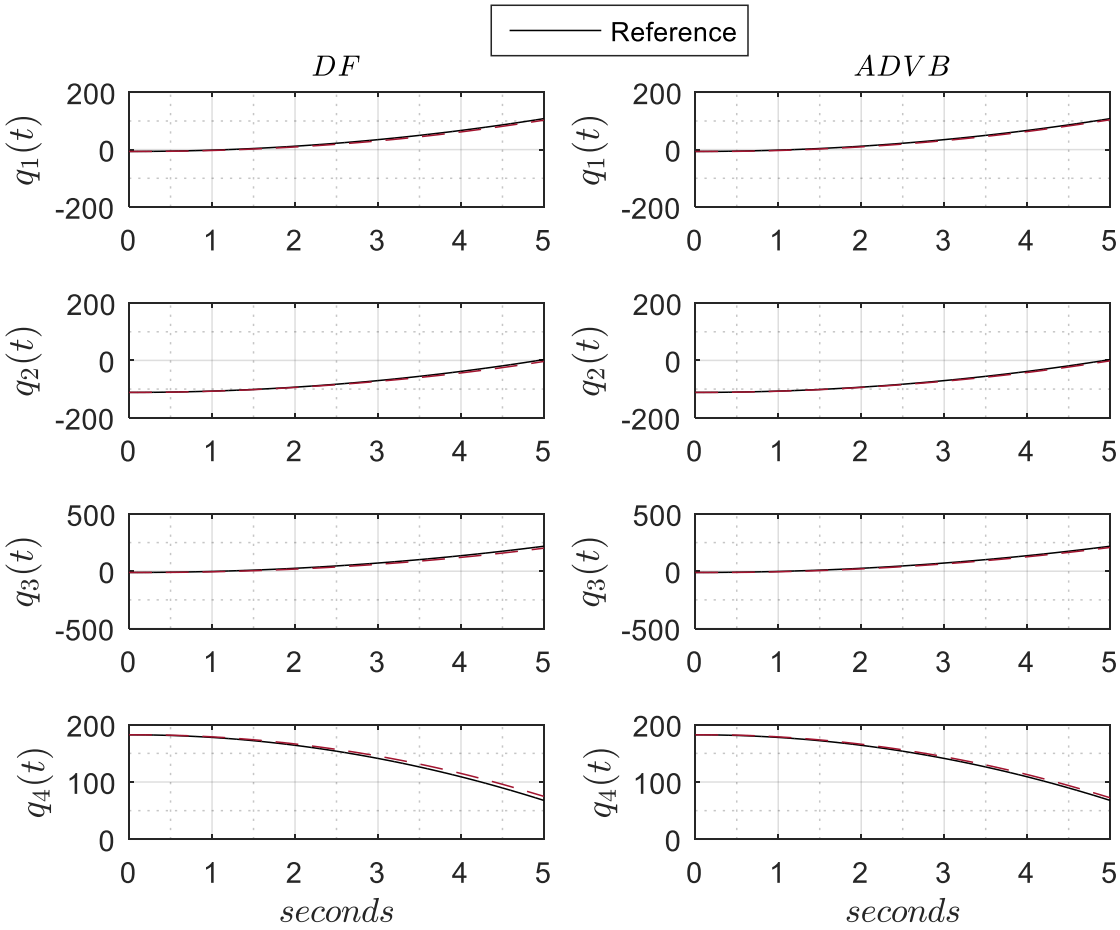

Figure 14. Plot of Joint Angles for SMC Integrated with DF (Left) for $a_i = 11$ and ADVB (Right)

By examining the overall performance reflected in Table III, Fig. 14 and Fig. 15, we observe that:

- The ADVB outperforms the DF. In particular, when the average tracking error across all joints is considered, ADVB errors are 28% smaller than those of the DF.
- The ADVB extends the performance of the SMC while preserving the smoothness of the torques, due to the smoothing characteristics of the filter.

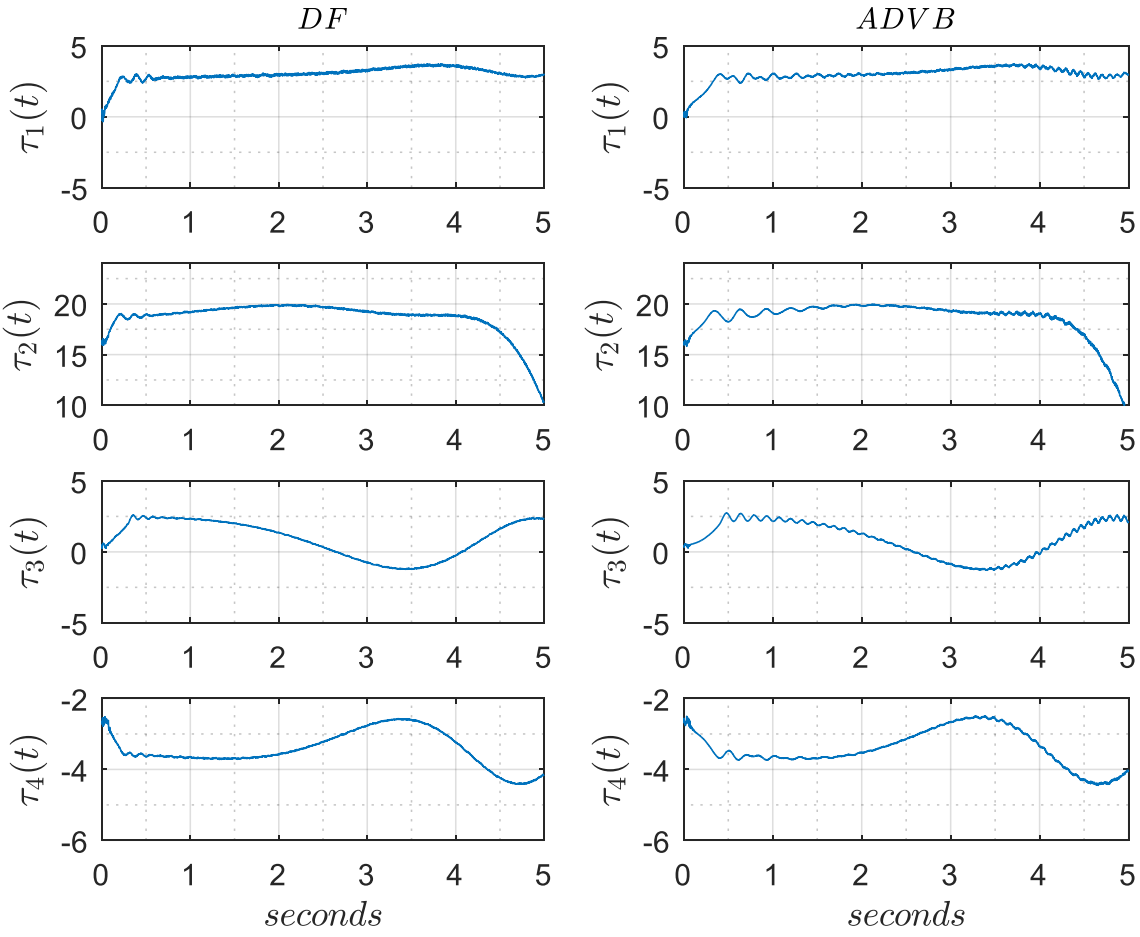

Figure 15. Plot of Joint Torques for SMC Integrated with DF (Left) for $a_i = 11$ and ADVB (Right)

5.5 Example 3

In this example, we first integrate the DF with the same SMC used in the numerical study. In order to illustrate the convex trend in performance exhibited by the DF, and as presented earlier, we vary the filter bandwidth and consider the average tracking performance across all joints for $a_i \equiv b_i = a \in \{3,..,10\}$, for $i \in \{1,..,4\}$.

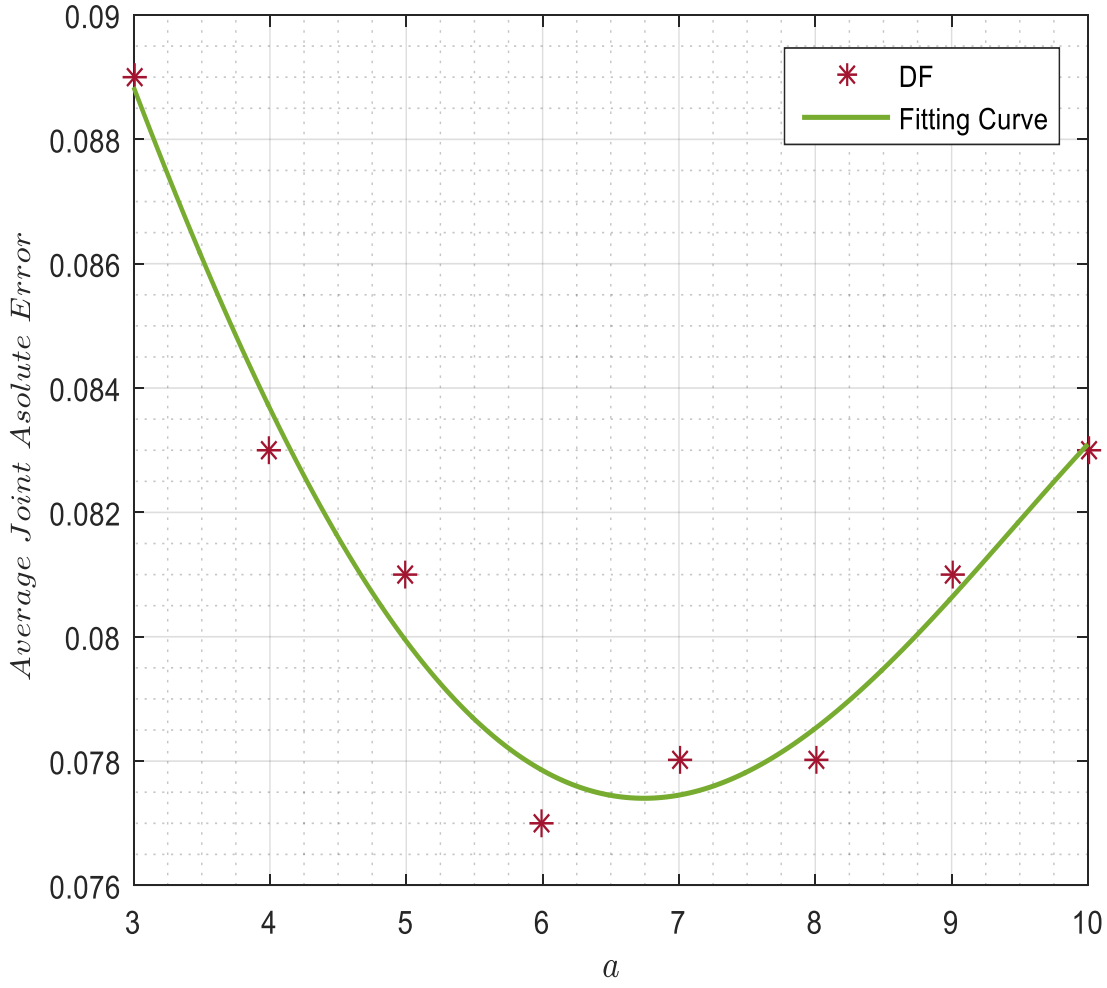

Figure 16. Average Joint Absolute Error of SMC with DF for different values of a

By examining the corresponding results in Fig. 16, we conclude the following:

- As the value of a increases, the average joint absolute error decreases and reaches a minimum value of 0.077 corresponding to $a = 6$, after which it consistently increases.
- The tracking performance exhibits a convex trend in function of the filter bandwidth a.
- As the value of a further increases beyond 10, the tracking performance keeps on decreasing, as expected.

Based on the previous results, we refer to the DF with $a = 6$ as the "optimal" DF. The goal is to illustrate how the proposed ADVB consistently improves the tracking performance when compared to the latter. For a consistent setup of DF and ADVB, we fix $a_i \equiv b_i = a = 6$ for the DF, and $a_i^r \equiv b_i^r = a^r = 3$ for the proposed ADVB, for $i \in \{1,..,4\}$. For the ADVB, we also consider different values of a_i^e as listed in Table IV. Fig. 17 plots the position angles of all joints while employing the "optimal" DF and the ADVB with $a^e = \text{diag}([500,800,500,500])$.

Table IV. Joint MAE for SMC Integrated with ADVB

ADVB Parameter $\boldsymbol{a^e}$	Joint 1	Joint 2	Joint 3	Joint 4	**Average**
$\boldsymbol{a_i^e = 500}$ $\forall\, \boldsymbol{i}$	0.050	0.043	0.076	0.050	**0.055**
$\boldsymbol{a_1^e = 500}$, $\boldsymbol{a_2^e = 800}$ $\boldsymbol{a_3^e = 500}$, $\boldsymbol{a_4^e = 500}$	0.049	0.035	0.076	0.051	**0.053**

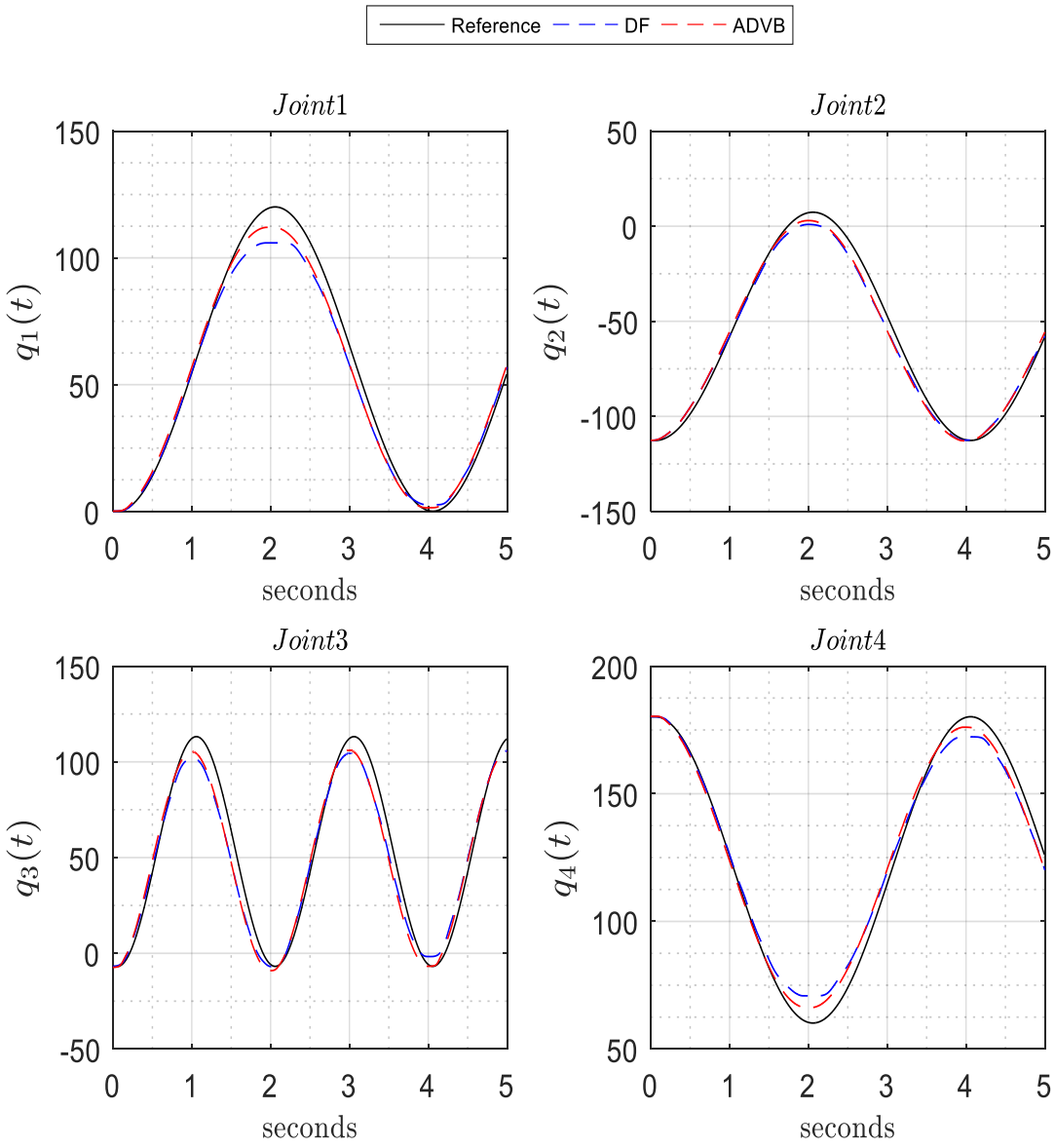

Figure 17. Joint Position for SMC integrated with "optimal" DF and ADVB

By examining the overall performance reflected in Table III and Fig. 12, we observe that:

- The ADVB always outperforms the "optimal" DF. In particular, when the average tracking error across all joints is considered, ADVB errors are 29% to 32% smaller than those of the "optimal" DF.

- The ADVB extends the performance of the SMC while preserving the smoothness of the torques, due to the smoothing characteristics of the filter.
- The tracking error of each joint can be individually controlled by varying its corresponding value in a^e.

Chapter 6

Conclusion

This research has shed some light on the characteristics of the discrete-time approximate differentiator filter (DF). Unlike its analog model, the discrete-time filter's bandwidth cannot be made arbitrarily large. It has been shown that such a filter shares the characteristics of an exponentially weighted moving average where the filter output is a *smooth* version of the derivative of its input. The integration of the filter with an SMC has been proposed and the stability analysis of the closed-loop system has been presented for a rigid robot manipulator. It has been shown that the employment of DF is more suitable than HGO for the system under consideration. Furthermore, it has been demonstrated that to preserve an *"optimal"* estimation performance, the filter bandwidth should be varied as the frequency of the filter input varies. Inspired by the latter, an approximate differentiator with varying bandwidth (ADVB) has been proposed, where the filter bandwidth varies based on the magnitude of the tracking position errors. Numerical and experimental validation has been presented on a 4 DOF robot arm. It has been shown that the proposed ADVB yielded 30% smaller tracking errors over an *"optimal"* DF.

Bibliography

[1] S. Spurgeon, "Sliding mode observers: a survey," *International Journal of Systems Science,* vol. 39, no. 8, pp. 751-764, 2008.

[2] U. Itkis, Control systems of variable structure, New York: Wiley, 1976.

[3] V. I. Utkin, "Variable structure systems with sliding modes," *IEEE Transactions on Automatic Control,* vol. 22, no. 2, pp. 212 - 222, 1977.

[4] V. I. Utkin, Sliding modes in control and optimization, Berlin: Springer-Verlag, 1992.

[5] G. Bartolini, A. Pisano, E. Punta and E. Usai, "A survey of applications of second-order sliding mode control to mechanical systems," *International Journal of control,* vol. 76, no. 9-10, pp. 875-892, 2003.

[6] F. Plestan, Y. Shtessel, V. Bre´geault and A. Poznyak, "New methodologies for adaptive sliding mode control," *International Joirnal of Control,* vol. 83, no. 9, p. 1907–1919, 2010.

[7] M. Defoort, T. Floquet, A. Kökösy and W. Perruquetti, "A novel higher order sliding mode control scheme," *Systems and Control Letters,* vol. 58, no. 2, pp. 102-108, 2009.

[8] X. Yu and O. Kaynak, "Sliding-mode control with soft computing: A survey," *IEEE Transactions on Industrial Electronics,* vol. 56, no. 9, pp. 3275 - 3285, 2009.

[9] J. Slotine and S. Sastry, "Tracking control of non-linear systems using sliding surfaces, with application to robot manipulators," *International Journal of Control,* vol. 38, no. 2, pp. 465-492, 1983.

[10] M. Zhang, Z. Yu, H. Huan and Y. Zhou, "The sliding mode variable structure control based on composite reaching law of active magnetic," *ICIC Express Letters,* vol. 2, no. 1, pp. 59-63, 2008.

[11] G. Bartolini, A. Ferrara and E. Usai, "Chattering avoidance by second-order sliding mode control," *IEEE Transactions on Automatic Control,* vol. 43, no. 2, pp. 241-246, 1998.

[12] R. Kikuuwe, S. Yasukouchi, H. Fujimoto and M. Yamamoto, "Proxy-based sliding mode control: A safer extension of PID position control," *IEEE Transactions on Robotics,* vol. 26, no. 4, pp. 670-683, 2010.

[13] Y. Orlov, J. Alvarez, L. Acho and L. Aguilar, "Global position regulation of friction manipulators via switched chattering control," *International Journal of Control,* vol. 76, no. 14, pp. 1446-1452, 2003.

[14] S. Purwar, "Higher order sliding mode controller for robotic manipulator," in *IEEE International Symposium on Intelligent Control*, Seville, 2007.

[15] A. Levant, "Higher-order sliding modes, differentiation and output-feedback control," *International Journal of Control,* vol. 76, no. 9-10, pp. 924-941, 2003.

[16] G. Rubio-Astorga, J. D. Sánchez-Torres, J. Cañedo and A. G. Loukianov, "High-order sliding mode block control of single-phase induction motor.," *IEEE Transactions on Control Systems Technology,* vol. 22, no. 5, pp. 1828-1836, 2014.

[17] D. Zhao, C. Li and Q. Zhu, "Low-pass-filter-based position synchronization sliding mode control for multiple robotic manipulator systems," *Proceedings of the Institution of Mechanical Engineers, Part I: Journal of Systems and Control Engineering,* vol. 225, no. 8, pp. 1136-1148, 2008.

[18] M. Tseng and M. Chen, "Chattering reduction of sliding mode control by low-pass filtering the control signal," *Asian Journal of control,* vol. 12, no. 3, pp. 392-398, 2010.

[19] M. Chen, Y. Hwang and M. Tomizuka, "A state-dependent boundary layer design for sliding mode control," *IEEE transactions on Automatic Control,* vol. 47, no. 10, pp. 1677-1681, 2002.

[20] M. Edardar, X. Tan and H. K. Khalil, "Design and analysis of sliding mode controller under approximate hysteresis compensation," *IEEE Transactions on Control Systems Technology,* vol. 23, no. 2, pp. 598-608, 2015.

[21] S. Tong and H.-X. Li, "Fuzzy adaptive sliding-mode control for MIMO nonlinear systems," *IEEE Transactions on Fuzzy Systems* , vol. 11, no. 3, pp. 354 - 360, 2003.

[22] Y. Huang, T. Kuo and S. Chang, "Adaptive sliding-mode control for nonlinearsystems with uncertain parameters," *IEEE Transactions on Systems, Man, and Cybernetics, Part B (Cybernetics),* vol. 38, no. 2, pp. 534-539, 2008.

[23] M. Li and Y. Chen, "Robust adaptive sliding mode control for switched networked control systems with disturbance and faults.," *IEEE Transactions on Industrial Informatics,* vol. 15, no. 1, pp. 193-204, 2019.

[24] Y. Feng, X. Yu and Z. Man, "Non-singular terminal sliding mode control of rigid manipulators," *Automatica,* vol. 38, no. 12, pp. 2159-2167, 2002.

[25] M. Zhihong, A. Paplinski and H. Wu, "A robust MIMO terminal sliding mode control scheme for rigid robotic manipulators," *IEEE transactions on Automatic Control,* vol. 39, no. 12, pp. 2464-2469, 1994.

[26] Y. Feng, X. Yu and F. Han, "On nonsingular terminal sliding-mode control of nonlinear systems," *Automatica,* vol. 49, no. 6, pp. 1715-1722, 2013.

[27] C. C. De Wit and N. Fixot, "Adaptive control of robot manipulators via velocity estimated feedback," *IEEE Transactions on Automatic Control,* vol. 37, no. 8, pp. 1234 - 1237, 1992.

[28] J. Slotine and L. Weiping, "Adaptive manipulator control: A case study," *IEEE Transactions on Automatic Control,* vol. 33, no. 11, pp. 995 - 1003, 1988.

[29] S. Nicosia and P. Tomei, "Robot control by using only joint position measurements," *IEEE Transactions on Automatic Control,* vol. 35, no. 9, pp. 1058 - 1061, 1990.

[30] S. Saab and P. Ghanem, "A multivariable stochastic tracking controller for robot manipulators without joint velocities," *IEEE Transactions on Automatic Control,* vol. 63, no. 8, pp. 2481-2495, 2018.

[31] H. Nemati, B. Bando and S. Hokamoto, "Chattering attenuation sliding mode approach for non-linear systems," *Asian Journal of Control,* vol. 19, no. 4, p. 1519–1531, 2017.

[32] R. H. Brown, S. C. Schneider and M. G. Mulligan, "Analysis of algorithms for velocity estimation from discrete position versus time data," *IEEE Transactions on industrial electronics,* vol. 39, no. 1, pp. 11-19, 1992.

[33] G. Liu, "On velocity estimation using position measurements," in *American Control Conference,* Anchorage, 2002.

[34] F. Janabi-Sharifi, V. Hayward and C. S. Chen, "Discrete-time adaptive windowing for velocity estimation," *IEEE Transactions on control systems technology,* vol. 8, no. 6, pp. 1003-1009, 2000.

[35] S. Jin, R. Kikuuwe and M. Yamamoto, " Improving velocity feedback for position control by using a discrete-time sliding mode filtering with adaptive windowing," *Advanced robotics,* vol. 28, no. 14, pp. 943-953, 2014.

[36] S.-H. Lee, T. Lasky and S. Velinsky, "Improved velocity estimation for low-speed and transient regimes using low-resolution encoders," *IEEE/ASME Transactions on Mechatronics,* vol. 9, no. 3, pp. 553-560, 2004.

[37] R. Kelly, "A simple set-point robot controller by using only position measurements," *IFAC Proceedings Volumes,* vol. 26, no. 2, pp. 527-530, 1993.

[38] H. Berghuis and H. Nijmeijer, "Global regulation of robots using only position measurements," *Systems & control letters,* vol. 21, no. 4, pp. 289-293, 1993.

[39] J. Shanhai, R. Kikuuwe and M. Yamamoto, "Discrete-time velocity estimator based on sliding mode and adaptive windowing," in *IEEE/SICE International Symposium on System Integration,* Fukuoka, 2012.

[40] J. Zhou, X. Shen, E. Petriu and N. Georganas, "Linear velocity and acceleration estimation of 3 DOF haptic interfaces," in *IEEE International Workshop on Haptic Audio visual Environments and Games,* 2008.

[41] S. Purwar, I. Kar and A. Jha, "Adaptive output feedback tracking control of robot manipulators using position measurements only," *Expert Systems with Applications,* vol. 34, no. 4, pp. 2789-2798, 2008.

[42] N. Cobanoglu, K. Cetin, E. Tatlicioglu and E. Zergeroglu, "A dynamic model free observer based output feedback tracking control of robot manipulators in task–space," in *American Control Conference*, Milwaukee, 2018.

[43] M. Farza, M. Oueder, R. B. Abdennour and M. M'Saad, "High gain observer with updated gain for a class of MIMO nonlinear systems," *International Journal of Control*, vol. 84, no. 2, pp. 270-280, 2011.

[44] J. Ahrens and H. Khalil, "High-gain observers in the presence of measurement noise: A switched-gain approach," *Automatica*, vol. 45, no. 4, pp. 936-943, 2009.

[45] R. G. Sanfelice and L. Praly, "On the performance of high-gain observers with gain adaptation under measurement noise," *Automatica*, vol. 47, no. 10, pp. 2165-2176, 2011.

[46] L. K. Vasiljevic and H. K. Khalil, "Differentiation with high-gain observers the presence of measurement noise," in *Proceedings of the 45th IEEE Conference on Decision and Control*, San Diego, 2006.

[47] H. Obeid, L. Fridman, S. Laghrouche, M. Harmouche and M. A. Golkani, "Adaptation of Levant's differentiator based on barrier function," *International Journal of Control*, vol. 91, no. 9, pp. 2019-2027, 2018.

[48] J. A. Moreno, "Exact differentiator with varying gains," *International Journal of Control*, vol. 91, no. 9, pp. 1983-1993, 2018.

[49] E. V. Nunes, L. Hsu and F. Lizarralde, "Arbitrarily small damping allows global output feedback tracking of a class of Euler-Lagrange systems," in *American Control Conference*, Washington, 2008.

[50] J. Moreno-Valenzuela, V. Santibanez, E. Orozco-Manrıquez and L. Gonzalez-Hernandez, "Theory and experiments of global adaptive output feedback tracking control of manipulators," *IET control theory & applications*, vol. 4, no. 9, pp. 1639-1654, 2010.

[51] J. Kirchhoff and O. Von Stryk, "Velocity estimation for ultralightweight tendon-driven series elastic robots," *IEEE Robotics and Automation Letters*, vol. 3, no. 2, pp. 664-671, 2018.

[52] B. Yao and M. Tomizuka, "Smooth robust adaptive sliding mode control of manipulators with guaranteed transient performance," in *American Control Conference*, Maryland, 1994.

[53] S. Islam and X. Liu, "Robust sliding mode control for robot manipulators," *IEEE Transactions on Industrial Electronics,* vol. 58, no. 6, pp. 2444-2453, 2011.

[54] B. Rahmani and M. Belkheiri, "Adaptive neural network output feedback control for flexible multi-link robotic manipulators," *International Journal of Control,* pp. 1-15, 2018.

[55] R. H. Jaafar and S. S. Saab, "Sliding Mode Control with Dirty Derivatives filter for rigid robot manipulators," in *IEEE Ubiquitous Computing, Electronics & Mobile Communication Conference*, New York, 2018.

[56] A. Loria, "Observers are unnecessary for output-feedback control of Lagrangian systems," *IEEE Transactions on Automatic Control,* vol. 61, no. 4, pp. 905-920, 2016.

[57] J. Lucas and M. Saccucci, "Exponentially weighted moving average control schemes: properties and enhancement," *Technometrics,* vol. 32, no. 1, pp. 1-12, 1990.

[58] V. Parra-Vega, S. Arimoto, Y.-H. Liu, G. Hirzinger and P. Akella, "Dynamic sliding PID control for tracking of robot manipulators: theory and experiments," *IEEE Transactions on Robotics and Automation,* vol. 19, no. 6, pp. 967-976, 2003.

[59] "WAM component list," Barret Technology Inc., 2013. [Online]. Available: http://support.barrett.com/wiki/WAM/SystemComponentList.

[60] "Kinematics, transmission rations, and joint ranges," Barret Technology Inc., 2013. [Online]. Available: http://support.barrett.com/wiki/WAM/KinematicsJointRangesConversionFactors.

[61] Z. Lu, S. Kawamura and A. A. Goldenburg, "An approach to sliding mode-based impedance control," *IEEE transactions on robotics and automation*, vol. 11, no. 5, pp. 754-759, 1995.

[62] J. Heredia and W. Yu, "A high-gain observer-based PD control for robot manipulator," in *Proceedings of the American Control Conference*, Chicago, 2000.